ARTICLE

SPRED2 loss-of-function causes a recessive Noonan syndrome-like phenotype

Marialetizia Motta,[1] Giulia Fasano,[1,18] Sina Gredy,[2,18] Julia Brinkmann,[3,18] Adeline Alice Bonnard,[4,5,18] Pelin Ozlem Simsek-Kiper,[6] Elif Yilmaz Gulec,[7] Leila Essaddam,[8] Gulen Eda Utine,[6] Ingrid Guarnetti Prandi,[9] Martina Venditti,[1] Francesca Pantaleoni,[1] Francesca Clementina Radio,[1] Andrea Ciolfi,[1] Stefania Petrini,[10] Federica Consoli,[11] Cédric Vignal,[4] Denis Hepbasli,[2] Melanie Ullrich,[2] Elke de Boer,[12,13] Lisenka E.L.M. Vissers,[12,13] Sami Gritli,[14] Cesare Rossi,[15] Alessandro De Luca,[11] Saayda Ben Becher,[8] Bruce D. Gelb,[16] Bruno Dallapiccola,[1] Antonella Lauri,[1] Giovanni Chillemi,[9,17] Kai Schuh,[2,19] Hélène Cavé,[4,5,19] Martin Zenker,[3,19] and Marco Tartaglia[1,*]

Summary

Upregulated signal flow through RAS and the mitogen-associated protein kinase (MAPK) cascade is the unifying mechanistic theme of the RASopathies, a family of disorders affecting development and growth. Pathogenic variants in more than 20 genes have been causally linked to RASopathies, the majority having a dominant role in promoting enhanced signaling. Here, we report that SPRED2 loss of function is causally linked to a recessive phenotype evocative of Noonan syndrome. Homozygosity for three different variants—c.187C>T (p.Arg63*), c.299T>C (p.Leu100Pro), and c.1142_1143delTT (p.Leu381Hisfs*95)—were identified in four subjects from three families. All variants severely affected protein stability, causing accelerated degradation, and variably perturbed SPRED2 functional behavior. When overexpressed in cells, all variants were unable to negatively modulate EGF-promoted RAF1, MEK, and ERK phosphorylation, and time-course experiments in primary fibroblasts (p.Leu100Pro and p.Leu381Hisfs*95) documented an increased and prolonged activation of the MAPK cascade in response to EGF stimulation. Morpholino-mediated knockdown of *spred2a* and *spred2b* in zebrafish induced defects in convergence and extension cell movements indicating upregulated RAS-MAPK signaling, which were rescued by expressing wild-type SPRED2 but not the SPRED2^{Leu381Hisfs*95} protein. The clinical phenotype of the four affected individuals included developmental delay, intellectual disability, cardiac defects, short stature, skeletal anomalies, and a typical facial gestalt as major features, without the occurrence of the distinctive skin signs characterizing Legius syndrome. These features, in part, characterize the phenotype of *Spred2*$^{-/-}$ mice. Our findings identify the second recessive form of Noonan syndrome and document pleiotropic consequences of SPRED2 loss of function in development.

Introduction

Dysregulated signaling through the RAS/mitogen-activated protein kinase (MAPK) cascade has profound consequences on cell behavior and development. Impaired function of the three members of the RAS subfamily or each tier of the MAPK backbone (i.e., RAF, MEK, and ERK proteins) dramatically affects cell homeostasis[1,2] and perturbs developmental programs.[3–7] On the other hand, enhanced or prolonged activation of this cascade due to activating variants in *HRAS* (MIM: 190020), *KRAS* (MIM: 190070), *NRAS* (MIM: 164790), *BRAF* (MIM: 164757), *RAF1* (MIM: 164760), *MAP2K1* (MIM: 176872), *MAP2K2* (MIM: 601263), or *MAPK1* (MIM: 176948) and an increasing number of genes encoding proteins acting as positive regulators of this signaling cascade is a major event contributing to oncogenesis and causes a family of diseases affecting development and growth collectively known as the RASopathies.[8–11] Equivalent consequences have been associated with loss-of-function (LoF) variants affecting negative regulators causing defective signaling switch-off.[12–15]

In line with the shared pathogenesis and the pleiotropic consequences of aberrant RAS/MAPK signaling in

[1]Genetics and Rare Diseases Research Division, Ospedale Pediatrico Bambino Gesù, IRCCS, 00146 Rome, Italy; [2]Institute of Physiology, University of Wuerzburg, 97070 Wuerzburg, Germany; [3]Institute of Human Genetics, University Hospital Magdeburg, 39120 Magdeburg, Germany; [4]Assistance Publique des Hôpitaux de Paris (AP-HP), Hôpital Robert Debré, Département de Génétique, 75019 Paris, France; [5]INSERM UMR 1131, Institut de Recherche Saint-Louis, Université de Paris, Paris, France; [6]Department of Pediatric Genetics, Hacettepe University Faculty of Medicine, Sihhiye, 06100 Ankara, Turkey; [7]Department of Medical Genetics, Health Sciences University, Istanbul Kanuni Sultan Suleyman Training and Research Hospital, 34303 Istanbul, Turkey; [8]Department of Pediatrics-PUC, Béchir Hamza Children's Hospital, Faculty of Medicine, University of Tunis El Manar, Jebbari 1007, Tunis, Tunisia; [9]Dipartimento per la Innovazione nei Sistemi Biologici, Agroalimentari e Forestali, Università Della Tuscia, 01100 Viterbo, Italy; [10]Confocal Microscopy Core Facility, Ospedale Pediatrico Bambino Gesù, 00146 Rome, Italy; [11]Medical Genetics Division, Fondazione IRCCS Casa Sollievo della Sofferenza, 71013 San Giovanni Rotondo, Italy; [12]Department of Human Genetics, Radboudumc, 6525 GA Nijmegen, the Netherlands; [13]Donders Institute for Brain, Cognition and Behaviour, Radboud University, 6525 GA Nijmegen, the Netherlands; [14]Department of Immunology, Pasteur Institute of Tunis, 1002 Tunis-Belvédère, Tunisia; [15]Genetica Medica, IRCCS Azienda Ospedaliero-Universitaria di Bologna, 40138 Bologna, Italy; [16]Mindich Child Health and Development Institute and Department of Pediatrics, Icahn School of Medicine at Mount Sinai, New York, NY 10029, USA; [17]Istituto di Biomembrane, Bioenergetica e Biotecnologie Molecolari, Centro Nazionale Delle Ricerche, 70126 Bari, Italy
[18]These authors contributed equally
[19]These authors contributed equally
*Correspondence: marco.tartaglia@opbg.net
https://doi.org/10.1016/j.ajhg.2021.09.007.

development, RASopathies are multisystem disorders with significant clinical overlap. Major features include a distinctive facies, postnatally reduced growth, a wide spectrum of congenital heart defects (CHD), hypertrophic cardiomyopathy (HCM), cognitive impairment and behavioral anomalies, skeletal and skin features, as well as variable predisposition to malignancies.[8,10,16,17] These disorders are generally transmitted as dominant traits, although recessive inheritance has recently been recognized in Noonan syndrome (NS [MIM: PS163950]),[18,19] the most clinically variable condition among RASopathies. While all RASopathies are rare disorders, NS and neurofibromatosis type 1 (NF1 [MIM: 162210]) are relatively common, which is likely due to the underlying genetic heterogeneity (NS), large size of the implicated gene (NF1), relatively mild impact on fitness (i.e., a significant proportion of families segregating the two disorders), and the selfish behavior of mutations in spermatogonial stem cells.[8,10,20]

Pathogenic variants in more than 20 genes have been reported to cause RASopathies.[21–24] Among these, only a minority (i.e., *CBL* [MIM: 165360], *LZTR1* [MIM: 600574], *NF1* [MIM: 613113], and *SPRED1* [MIM: 609291]) encode proteins functioning as negative modulators of the RAS-MAPK pathway. In this context, inefficient signaling switch-off operating at the level of RAS proteins has been established as the mechanism of disease underlying NF1 and Legius syndrome (LGSS [MIM: 611431]).[25] NF1 is characterized by Lisch nodules on the iris, cutaneous *café-au-lait* macules (CALMs), axillary/inguinal freckling, skeletal defects, learning disabilities, neurofibromas, and increased risk for certain cancers (Table S1).[26] The disorder is caused by heterozygous inactivating variants in *NF1*, which encodes neurofibromin, a multidomain protein functioning as a RAS-specific GTPase activating protein (GAP) negatively controlling RAS activity by promoting conversion of active GTP-bound RAS to its inactive, GDP-bound state.[27,28] Of note, a small proportion of subjects with pathogenic *NF1* variants shows clinical overlap with NS, resulting in the so-called neurofibromatosis-Noonan syndrome (MIM: 601321).[29,30] Similar to NF1, LGSS is characterized by CALMs, with or without freckling; in LGSS, however, Lisch nodules and the NF1-associated neurofibromas and malignancies do not occur (Table S1).[31] In affected subjects, developmental delay (DD), behavioral anomalies, and hyperactivity, as well as facial features suggestive of NS are commonly reported. The disorder is caused by heterozygous mutations in the Sprouty-related, EVH1 domain containing 1 (*SPRED1*) gene,[32] encoding a protein inhibiting RAS function by promoting neurofibromin translocation to the plasma membrane and its binding to GTP-bound RAS.[33,34] SPRED binding to neurofibromin is a required step for the ability of the GAP to suppress RAS function, and a recent study has solved the structure of the ternary complex involving SPRED1, neurofibromin, and GTP-bound KRAS, providing mechanistic insights of this regulatory circuit negatively controlling RAS-MAPK signaling.[34]

The three members of the SPRED family (i.e., SPRED1, SPRED2, and SPRED3) share a similar domain organization and function.[25,35] These proteins are characterized by an *N*-terminal Enabled/VASP homology 1 (EVH1) domain, a central c-Kit related binding domain (KBD) (missing in SPRED3), and a C-terminal cysteine-rich Sprouty-related (SPR) domain. The EVH1 domain is essential for the inhibitory function of SPRED proteins exerted on RAS since it mediates binding of the protein to neurofibromin.[34,36] The SPR domain, which is shared with the members of the Sprouty family, undergoes post-translational processing (i.e., palmitoylation) and is responsible for binding of SPRED proteins to the cytoplasmic leaflet of membranes.[37–39] The three proteins negatively regulate signal traffic through the RAS-MAPK pathway elicited by multiple growth factors (e.g., FGF and EGF) and cytokines, with SPRED1 and SPRED2 sharing the stronger suppression activity.[39] Of note, partial redundancy in Spred1 and Spred2 function has been documented.[40]

Despite the successful use of exome/genome sequencing in understanding the molecular bases of RASopathies during the last years, a large proportion of individuals with a clinical diagnosis of RASopathy or having an unclassified but RASopathy-related phenotype remains molecularly unsolved. By a "functional candidacy" strategy performed in the frame of the NSEuroNet consortium, using parallel sequencing of a panel of genes functionally related to the currently known RASopathy genes, we identify *SPRED2* (MIM: 609292) as a gene implicated in a RASopathy clinically resembling NS. Biochemical, *in vitro* and *in vivo* functional studies indicate that the identified *SPRED2* variants are inactivating and that SPRED2 LoF results in an enhanced, stimulus-dependent activation of the MAPK cascade. Remarkably and differently from LGSS, this new condition is transmitted as a recessive trait, indicating a differential requirement of SPRED2 and SPRED1 function in developmental processes.

Material and methods

Subjects

Subjects from three unrelated consanguineous families were included in the study. Clinical data, DNA samples, and skin biopsies were collected from the participating families after written informed consent was obtained. DNA samples and primary fibroblast lines were collected, stored, and used following procedures in accordance with the ethical standards of the declaration of Helsinki protocols, under research projects approved by the Review Boards of the participating institutions (Ospedale Pediatrico Bambino Gesù, Rome; Otto von Guericke University, Magdeburg; CHU Hôpital Robert Debré, Paris). Explicit permission was obtained to publish the photographs of the subjects shown in Figure 1. The additional RASopathy cohorts included in the study were referred for diagnostic genetic testing because of a suspected RASopathy.

Figure 1. Clinical features and pedigrees of the subjects with bi-allelic inactivating *SPRED2* variants
(A) Facial features of the four individuals included in this study. Note the occurrence of bitemporal narrowing, hypertelorism, downslanting palpebral fissures, ptosis, low-set/posteriorly rotated ears with evident antitragus, wide nasal bridge, and low posterior hairline with a webbed/short neck. Typical NS chest anomalies (superior pectus carinatum and inferior pectus excavatum) are also evident. Craniofacial features resemble NS. The NS facial gestalt is particularly represented in subject 2-II-1.
(B) Pedigree charts of the three families with bi-allelic inactivating *SPRED2* variants. All probands were born from first cousins. Note the high inbreeding of family 1.

Molecular analyses

Mutation scan of the known genes implicated in RASopathies and a selected panel of candidates was performed at the reference centers for RASopathy testing of the Robert Debré University Hospital (Paris, France), Magdeburg University Hospital (Magdeburg, Germany), Ospedale Pediatrico Bambino Gesù (Rome, Italy), Policlinico S. Orsola (Bologna, Italy), and Fondazione IRCCS Casa Sollievo della Sofferenza (San Giovanni Rotondo, Italy). The panels used included *PTPN11* (MIM: 176876), *CBL*, *SOS1* (MIM: 182530), *SOS2* (MIM: 601247), *HRAS*, *KRAS*, *NRAS*, *RIT1* (MIM: 609591), *RRAS* (MIM: 165090), *RRAS2* (MIM: 600098), *MRAS* (MIM: 608435), *NF1*, *SPRED1*, *LZTR1*, *SHOC2* (MIM: 602775), *PPP1CB* (MIM: 600590), *RAF1*, *BRAF*, *MAP2K1*, *MAP2K2*, *SPRED2*, and a variable additional list of candidates. Enrichment of target genes was achieved using a Nextera Rapid Capture Custom Enrichment kit (Illumina) (Magdeburg), SureSelectQXT target enrichment system (Agilent) (Paris, San Giovanni Rotondo), and multiplex PCR using an Ion AmpliSeq On-Demand panel (ThermoFisher Scientific) (Bologna). In all analyses, a minimum depth of 100× for all target regions was generally attained (>20×, Paris; >200× Magdeburg). Alignment and variant calling were performed with the MiSeq Reporter software (Illumina), followed by annotation of VCF output files using Variant Studio v.2.2 (Illumina) (Magdeburg, San Giovanni Rotondo), Ion Reporter Software (ThermoFisher Scientific) (Bologna), or BenchlabNGS Alissa Interpret v.5.2 (Agilent) (Paris). All reported variants were visualized with the Integrative Genomics Viewer v.2.3 or Alamut Visual v.2.15 software.

Exome sequencing (trio-based approach) was performed using DNA samples obtained from peripheral blood leukocytes. Target enrichment was performed using the SureSelect Clinical Research Exome v.2 and SureSelect Exome v.7 (Agilent). WES data processing, including sequence alignment to GRCh37 or GRCh38, and variant filtering and prioritization by allele frequency, predicted functional impact, and inheritance were performed as previously reported.[24,41,42]

Structural modeling analysis

Structural analyses used the recently solved structure of the complex in which the neurofibromin GAP-related domain (GRD) interacts with the EVH1 domain of SPRED1 and GTP-bound KRAS (PDB: 6v65) as a template,[34] by using the SWISS-MODEL automated protein structure homology modeling server.[43] The 3-dimensional structure was visualized using the VMD visualization software.[44] The structural impact of the p.Leu100Pro change was explored using the UCSF Chimera package.[45] The side-chain orientations were obtained with the Dunbrack backbone-dependent rotamer library,[46] choosing the best rotamer with minimal/no steric clashes with neighboring residues.

Reagents and expression constructs

Dulbecco's modified Eagle's medium (DMEM), fetal bovine serum (FBS), phosphate-buffered saline (PBS), glutamine, and antibiotics were obtained from Euroclone. Fugene6 transfection reagent and complete protease inhibitor cocktail tablets were purchased from Roche Diagnostics. Epidermal growth factor (EGF) was from Invitrogen. Cycloheximide (CHX), MG132, and Bafilomycin A1 were from Sigma-Aldrich. Protein G Sepharose was obtained from GE Healthcare. Trans-Blot Turbo Transfer Packs were from Bio-Rad Laboratories. ECL Western Blotting Detection reagents were purchased from Pierce Biotechnology. Alexa Fluor 488 phalloidin dye was from Molecular Probes. Vectashield anti-fade medium containing DAPI was purchased from Vector Laboratories. The following antibodies were used: mouse monoclonal IgG1 anti-Xpress and mouse monoclonal IgG2a anti-V5 (Invitrogen); rabbit polyclonal anti-GAPDH (zebrafish) (Genetex); rabbit monoclonal GM130 (Abcam); mouse monoclonal anti-neurofibromin (H12) and mouse monoclonal anti-GAPDH (Santa Cruz Biotechnology); rabbit polyclonal anti-p44/42 ERK1/2 (MAPK3/1), mouse monoclonal anti-phospho-p44/42 ERK1/2 (MAPK3/1) (Thr202/Tyr204), mouse monoclonal anti-MEK1/2, and rabbit polyclonal anti-phospho-MEK1/2 (Ser217/221) (Cell Signaling Technology); rabbit polyclonal anti-RAF1 (Abcam); mouse monoclonal anti-phospho-RAF1 (Ser338) (Millipore); horseradish peroxidase-conjugated anti-rabbit or anti-mouse (Sigma-Aldrich); goat anti-mouse IgG conjugated to Alexa Fluor 594 and Alexa Fluor 488, goat anti-mouse IgG1 and goat anti-mouse IgG2a conjugated to Alexa Fluor 647 and Alexa Fluor 594, respectively, and goat anti-rabbit conjugated to Alexa Fluor 594 (Molecular Probes).

The entire *SPRED2* and *LZTR1*, and neurofibromin GRD coding sequences were cloned into the pcDNA6/Xpress-HisC, pcDNA6.2/V5-DEST and pcDNA6/V5-HisA eukaryotic expression vectors (Invitrogen), respectively. Mutations were introduced using

primed amplification by polymerase chain reaction (site-directed mutagenesis) using the QuiKChange II Site-Directed Mutagenesis kit (Stratagene), as previously described.[47] All constructs were bidirectionally Sanger-sequenced for their entire open reading frame.

Cell culture, transfection, inhibitor treatment, and EGF stimulation

COS-1, HEK293T (ATCC), and fibroblast cells were maintained in DMEM medium supplemented with 10% heat-inactivated FBS, 1% L-glutamine, and antibiotics. Sub-confluent cells were transfected using the Fugene6 transfection reagent according to the manufacturer's instructions. Cells were treated with CHX (10 μg/mL), MG132 (50 μM), or Bafilomycin A1 (200 nM) to assess protein stability and degradation pathways. Serum-free DMEM and EGF were utilized to starve and stimulate cells, respectively.

Cell homogenate and protein assays

Cells were lysed in radio-immune precipitation assay (RIPA) buffer (pH 8.0) containing 20 mM NaF, 1 mM Na_3VO_4, and protease inhibitors. Lysates were kept on ice for 30 min and then centrifuged at 16,000 × *g* for 20 min at 4°C. Supernatants were collected and their protein concentration was determined by the bicinchoninic acid assay,[48] using bovine serum albumin as a standard.

Immunoblotting

Assays were as previously reported.[47] In brief, cell lysates were resolved by sodium dodecyl sulfate (SDS)-polyacrylamide gel. After electrophoresis, proteins were transferred to a nitrocellulose membrane using the Trans-Blot Turbo transfer system. Blots were blocked with 5% non-fat milk powder in PBS containing 0.1% Tween-20 for 1 h and incubated with specific antibodies overnight (pRAF1/MEK/ERK and coimmunoprecipitation assays) or for 1 h (SPRED2 level analyses). Primary and secondary antibodies were diluted in blocking solution. Immunoreactive proteins were detected by an enhanced chemiluminescence (ECL) detection kit. Densitometric analysis of protein bands was performed using NineAlliance UVITEC software (UVITEC).

RAF1, MEK, and ERK phosphorylation assays

RAF1, MEK, and ERK phosphorylation assays were performed on transfected HEK293T cells seeded in 6-well plates the day before transfection (70%–80% confluence) and on sub-confluent primary fibroblasts. Cells were serum-starved for 16 h and then stimulated with EGF (transfected cells: 30 ng/mL, assessed 5 and 10/15 min after stimulation; primary fibroblasts: 10 ng/mL, assessed 15, 30, and 60 min after stimulation) or left unstimulated.

Confocal laser scanning microscopy

For subcellular localization analyses, COS-1 cells were seeded at the density of 1.5×10^4 in 24-well cluster plates onto 12-mm coverslips. After 24 h of culture in complete medium, cells were transfected with the indicated constructs. At 24 h after transfection, cells were treated with bafilomycin A1 (200 nM, 4 h) or left untreated and fixed with 3% paraformaldehyde. For GRD-SPRED2 co-localization analysis, transfected COS-1 cells were serum-starved for 16 h and then stimulated with EGF (30 ng/mL, 5 min). Fixed cells were permeabilized with 0.5% Triton X-100 and stained with a mouse monoclonal IgG1 anti-Xpress followed by goat anti-mouse IgG1 Alexa Fluor 647 (SPRED2 in SPRED2-neurofibromin GRD co-localization assays) or goat anti-mouse IgG Alexa Fluor 594 (SPRED2 localization) and then with Alexa Fluor 488 phalloidin dye or using a mouse monoclonal IgG2a anti-V5 followed by goat anti-mouse IgG2a Alexa Fluor 594 (GRD in SPRED2-neurofibromin GRD co-localization assays) or goat anti-mouse IgG Alexa Fluor 488 (V5-tagged LZTR1) and a rabbit monoclonal GM130 followed by goat anti-rabbit IgG Alexa Fluor 594. After staining, coverslips were extensively rinsed and then mounted on the microscope slides by using Vectashield with DAPI mounting medium. Confocal analysis was performed by a Leica TCS-SP8X (Leica Microsystems) equipped with a 405 nm diode laser and a white light laser (WLL) source using excitation spectral laser lines at 488 nm, 594 nm, and 647 nm. Cells stained only with the fluorochrome-conjugated secondary antibody were used to set up acquisition parameters. Signals from different fluorescent probes were taken in sequential scanning mode. Image processing used Adobe Photoshop 7.0 software (Adobe Systems Incorporated).

Co-immunoprecipitation assays

HEK293T cells transfected with WT or variant *SPRED2* constructs were serum-starved, stimulated with EGF (30 ng/mL), and lysed in IP buffer containing 25 mM Tris–HCl (pH 7.4), 1% Triton X-100, 2 mM EDTA (pH 8.0), 150 mM NaCl, and protease inhibitors. Samples were centrifuged at 10,000 × *g* (20 min, 4°C), supernatants were collected, and equal amounts of total proteins were immunoprecipitated using an anti-Xpress antibody cross-linked to Protein G Sepharose beads (2 h, 4°C). The beads were recovered by centrifugation and washed six times with IP buffer. Finally, the immunoprecipitated proteins were eluted with sample buffer by incubating at 95°C (5 min) and stored at −20°C until western blot (WB) analysis (WT SPRED2, 10 μL; mock, 30 μL; $SPRED2^{Leu100Pro}$, 30 μL), due to the accelerated degradation of the variant. Immunoprecipitated endogenous neurofibromin was normalized to the amount of the relative immunoprecipitated SPRED2 proteins.

Zebrafish studies

Zebrafish were cultured following standard protocols.[49] Fish were housed in a water circulating system (Tecniplast) under controlled conditions (light/dark 14:10 h, 28°C, 350–400 uS, pH 6.8–7.2) and fed daily with dry and live (*A. salina*) food. All the experimental protocols were approved by the Italian Ministry of Health (23/2019-PR).

Embryos were obtained from natural mating of NHGRI pairs.[50] Selected pairs did not carry variation within the 24-nucleotide stretch targeted by the designed ATG-morpholino (MO) sequences (Figure S1). Co-injection of *spred2a* and *spred2b* ATG-MOs targeting both *spred2a* and *spred2b* (6 ng) was performed at the 1-cell stage. Co-injection of p53 ATG-MO was used to control for p53-dependent neural toxicity.[51,52] Wild-type (WT) and variant (p.Leu381Hisfs*95) *SPRED2* sequences were cloned into a pCS-Dest vector (gift from Nathan Lawson, plasmid 22423, Addgene) via LRII clonase-mediated recombination (ThermoFisher). Plasmids were digested and linearized with *Kpn*I (New England Biolabs), and mRNA was produced using mMessage mMachine SP6 transcription kit and poly(A) tailing kit (Thermo Fisher). All cloned sequences were confirmed by bidirectional Sanger sequencing.

Injection of *in vitro* synthesized capped mRNAs encoding *SPRED2* alleles (1.5 pg) was used in the rescue experiments. Injected embryos were cultured under standard conditions at 28°C in fresh E3 medium and non-injected fish were used as controls together with fish injected with individual *SPRED2* mRNAs. To

assess pErk levels in morphants, embryonic tissues (12 hpf) were homogenized in lysis buffer (10 mM Tris-HCl [pH 7.4], 2 mM EDTA, 150 mM NaCl, 1% Triton X-100) supplemented with protease inhibitors. Following centrifugation (20,000 × *g*, 10 min, 4°C), supernatants were collected and protein concentration was determined by Bradford assay (Bio-Rad). WB analysis was performed as reported above. At the end of gastrulation (12 hpf), embryos were imaged using a Leica M205 stereomicroscope. For the phenotype penetrance analysis of zebrafish morphants, fully developed embryos without recognizable defects were classified as "normal," embryos showing mild developmental delay within the segmentation period (10–11 hpf) as "mild," and embryos showing developmental arrest in any phase of gastrula period (epiboly between 60%–90%) as "severe." Only "normal" and "mild" subgroups were considered for major and minor axes measurements. The axes of the embryos and the elongation ratio (major-to-minor) were measured and calculated using Fiji.[53] Data were analyzed independently by two researchers, and statistical assessments were performed using GraphPad Prism. Normality tests (Anderson-Darling, D'Agostino & Pearson, Shapiro-Wilk, and Kolmogorov-Smirnov tests) were run to assess the normal distribution of the data. Two-tailed Fisher exact test was used to assess the statistical significance of phenotypes in morphants (2×2 contingency table). For the elongation analysis, one-way ANOVA with two-stage Benjamini, Krieger, and Yekutieli procedure was run for controlling the false discovery rate of multiple comparisons; Student's t test was used to assess the statistical significance of pErk levels in morphants.

Spred2 knock-out mouse phenotyping

Spred2$^{-/-}$ mice were raised by crossbreeding heterozygous *Spred2*$^{+/-}$ mice derived from the embryonic stem cell clone XB228 (BayGenomics RRID: CVCL_PG99). To avoid inbreeding effects, only mice of a mixed 129/Ola × C57BL/6 outbred background at the indicated ages were used. All procedures involving animals were in accordance with European guidelines (2010/63/EU) and were approved by the government of Lower Franconia.

For electrocardiographic (ECG) recordings, mice were anesthetized using 1.5% isoflurane and kept on a warming plate (37°C) throughout the experiment. ECGs were captured at a sampling rate of 4,000 points per second using a PowerLab 8/35 system equipped with BIOamplifiers (ADInstruments) for 10 min, and original ECG recordings were analyzed with the ECG analysis module of LabChart Pro 8.1.8 (ADInstruments).

To quantify the relative volumes of the brain ventricle system, 100-μm sections were cut from perfusion-fixed brains using a VT1000S vibratome (Leica). Individual brain slices were photographed and the background removed. In the resulting images, the ventricle areas were measured using ImageJ (https://imagej.nih.gov). Volumes were calculated using the original slice thickness of 100 μm. Relative volumes were calculated in relation to whole brain volumes. The three-dimensional brain models were compiled with ImageJ and visualized with Imaris (Oxford Instruments). To investigate hippocampus formation, 10-μm-thick brain sections were stained according to the standard Nissl staining procedure. Levels of Spred2 were assessed using a polyclonal rabbit anti-Spred2 antibody (residues 96–415).[54] To assess Ras activity, hippocampus regions were dissected from mouse brains on a metal plate cooled with ice and homogenized in an assay-dependent buffer using a plastic douncer fitting into a 1.5 mL microreaction tube. Pan-Ras Activation Assay Kit (#STA-400, Cell Biolabs) was used to detect active Ras, following the manufacturer's protocol. Fifty milligrams of tissue were lysed in 1 mL assay buffer and 1 mg total protein was used for each Ras pull-down. To investigate kidney morphology, 10 μm-thick paraffin-embedded kidney sections were stained according to the standard hematoxylin-eosin staining protocol.

Results

Bi-allelic variants in *SPRED2* cause a disorder resembling Noonan syndrome

Three probands (subjects 1-II-1, 2-II-1, and 3-II-1) suspected to be affected by NS or a related RASopathy were referred for diagnostic genetic testing (Figure 1A). The pedigrees of the three consanguineous families are shown in Figure 1B. Genomic DNA obtained from peripheral blood leukocytes was scanned for variations using an "extended" panel of RASopathy genes opportunely designed to include a set of candidate genes selected in the frame of the NSEuroNet consortium. In family 1, parallel sequencing in the proband identified a previously unreported frameshift variant in *SPRED2*, c.1142_1143delTT (p.Leu381Hisfs*95; GenBank: NM_181784.2) in homozygosity, affecting the C terminus of the protein, a region highly intolerant for variation (Figure S2). The variant was predicted to result in a longer open reading frame characterized by a divergent *C*-terminal tail lacking key cysteine residues required for proper SPRED2 post-translational processing and plasma membrane targeting (Figure S3). Segregation analysis confirmed homozygosity in the affected father (1-I-1) and heterozygosity in the apparently healthy mother. In family 2, analysis in the proband (2-II-1) identified a homozygous missense change (c.299T>C [p.Leu100Pro]), which was private and altered an invariantly conserved residue among orthologs and paralogs (Figure S3) located within a second highly constrained region of the protein (Figure S2). The variant was inherited by his apparently healthy consanguineous parents, who were confirmed to be heterozygous for the missense change. Of note, somatic mutations of this residue and the adjacent Gly^{99} have previously been reported in cancer (COSMIC database), and multiple pathogenic missense changes affecting the adjacent residue Thr^{101} in SPRED1 (p.Thr102Met/Lys/Arg) had causally been linked to LGSS,[55,56] supporting the functional and clinical relevance of the variant. In this subject, a homozygous condition for a missense variant in *LZTR1* (c.1856G>A [p.Arg619His]; GenBank: NM_006767.3) was also identified. This variant had been reported in public databases (rs568213908, ExAC 0.04%) and was classified as a variant of uncertain significance by ClinVar. *In silico* prediction tools consistently considered the missense change as tolerated (CADD [v.1.6, hg19] = 16.59; REVEL = 0.069; M-CAP = 0.012 [tolerated]; SIFT: tolerated; PolyPhen-2: benign). Arg^{619} is only moderately conserved, and His at the same codon is found in multiple mammalian species, suggesting that this missense change does not adversely

Table 1. Clinical features of subjects with bi-allelic pathogenic *SPRED2* variants

Case ID	1-II-1	1-I-1	2-II-1	3-II-1
Ethnicity	Turkish	Turkish	Turkish	Tunisian
Sex	female	male	male	female
Age at last examination	14 years 2 mo	39 years	8 years	11 years 11 mo
***SPRED2* variant**				
cDNA change (NM_181784.2)	c.1142_1143delTT	c.1142_1143delTT	c.299T>C	c.187C>T
AA change (NP_861449.2)	p.Leu381Hisfs*95	p.Leu381Hisfs*95	p.Leu100Pro	p.Arg63*
Inheritance	bi-allelic	bi-allelic	bi-allelic	bi-allelic
ExAC/gnomAD frequency	–	–	–	–
Growth at last examination	14 years 2 mo	39 years	8 years	11 years 11 mo
Height (SD)	145 cm (−2.41)	144 cm (−4.35)	122.2 cm (−1.00)	136.5 cm (−1.50)
Weight (SD)	42 kg (−1.02)	56 kg (−1.29)	22 kg (−1.09)	27.5 kg (−2.30)
Head circumference (SD)	57 cm (+1.32)	56 cm (−1.00)	51 cm (+0.86)	55 cm (+1.00)
Development				
Developmental delay	yes	yes (by history)	mild	no
Intellectual disability	mild	mild (by history)	mild	yes
Language delay	yes	yes	yes	no
Learning disorder	yes	yes (by history)	yes	attention deficit
Neurological features				
Hypotonia	yes	yes (by history)	during infancy	no
Cardiovascular features				
Congenital heart defect	yes (mild aortic insufficiency, mitral valve prolapse)	no	yes (pulmonary valve stenosis, pulmonary balloon valvuloplasty; small secundum ASD)	yes (pulmonary valve stenosis)
Hypertrophic cardiomyopathy	yes (focal interventricular septum hypertrophy)	yes	yes (asymmetrical hypertrophy of the interventricular septum)	no
Skeletal features				
Chest	pectus excavatum	pectus excavatum	pectus carinatum superiorly and pectus excavatum inferiorly; wide and short shield chest	pectus excavatum
Hyperlaxity	yes	no	yes	yes
Other skeletal anomalies	cubitus valgus	no	limited extension of elbows, cubitus valgus, winged shoulder blades, kyphosis, mild pes valgus and pes planus	kyphosis, clinodactyly, abnormal toe position
Facial features				
Bitemporal narrowing	yes	yes	yes	yes
Hypertelorism	yes	no	yes	yes
Low-set and/or posteriorly rotated ears	yes	yes	yes	yes
Prominent nasal bridge	yes	yes	yes	yes
Low posterior hairline	yes	yes	yes	yes

(*Continued on next page*)

Table 1. ***Continued***

Case ID	1-II-1	1-I-1	2-II-1	3-II-1
Short/webbed neck	yes	yes	yes	yes
Other dysmorphism or clinical features	helix folding anomaly, dysmorphic ear lobe	downward slanted palpebral fissures, prominent nasolabial folds, long philtrum	triangular coarse face, sparse eyebrows, sparse eyelashes, downward slanted palpebral fissures, epicanthus, nasolacrimal duct stenosis, prominent nasolabial sulci, pointed receding chin	high cranial vault, triangular and coarse face, downward slanted palpebral fissures, ptosis, prominent philtrum, large mouth, thick lips, micrognathia, high arched/ narrow palate
Skin				
Café-au-lait spots	no	no	no	no
Freckling	no	no	no	no
Other skin/ectodermal features	nevi	no	sparse and curly hair, sparse and thin eyebrows and eyelashes, scaly and dry skin, eczematous skin, loose and thick skin, deep palmar creases	hyperhydrosis, deep palmar creases
Other features/sign				
Cryptorchidism	N/A	no	bilateral	N/A
Lymphatic involvement	no	no	no	no
Bleeding/easy bruising	yes	no	partial FXII deficiency (24.8% activity)	no
Hematological abnormalities	lymphopenia	no	no	no
Other	no	tiny hemangiomas	atopic skin features, nasolacrimal duct stenosis, exotropia, bone pain and myalgia	transient splenomegaly that gradually disappeared between age 2.5 and 8.5 years, sigmoid dolichocolon
Imaging	brain MRI: mild left cerebral hemisphere enlargement	N/A	trans-fontanelle USG: left lateral ventriculomegaly; renal USG: bilateral grade 2 medullary nephrocalcinosis	N/A

affect protein function. To further confirm these predictions, the *LZTR1*^{Arg619His} cDNA was generated by site-directed mutagenesis, and functional characterization of the V5-tagged LZTR1 variant was assessed in terms of protein stability and subcellular localization and by evaluating its impact on pERK levels, which confirmed a behavior equivalent to the WT protein (Figure S4).[57] Finally, a previously unreported homozygous *SPRED2* nonsense change, c.187C>T, predicting protein truncation at the N terminus (p.Arg63*), was identified in subject 3-II-1, who had clinical features suggestive of NS. Parallel/Sanger sequencing confirmed the heterozygosity condition in the apparently unaffected sib and parents.

The clinical data of the four affected subjects from the three families are shown in Table 1, and their detailed clinical history is provided in the supplemental note (case reports). Shared features of the four affected individuals included DD/intellectual disability (ID), speech delay, and learning difficulties. Short stature (<−2 SD) with relative macrocephaly was documented in three individuals. Hypotonia was a common feature during childhood. Cardiac involvement occurred in all individuals. Specifically, HCM was documented in subject 1-I-1, asymmetrical interventricular septal hypertrophy and pulmonary valve stenosis (PVS) requiring balloon valvuloplasty was present in subject 2-II-1, and PVS occurred in subject 3-II-1. The distinctive craniofacial appearance included bitemporal narrowing (4/4 cases), hypertelorism (3/4 cases), ptosis (2/4 cases), down-slanting palpebral fissures (3/4 cases), low-set/posteriorly rotated ears (4/4 cases), prominent nasal bridge (4/4 cases), anteverted nares (3/4), long/prominent philtrum (3/4), and low posterior hairline with a webbed/ short neck (4/4 cases), which are observed as major features in RASopathies. Typical NS chest anomalies (pectus carinatum and/or excavatum) and other skeletal defects (spine) were also common findings. Cryptorchidism and bleeding diathesis occurred in single individuals. No lymphedema or skin/ectodermal anomalies were noted except for the occurrence of deep palmar creases (2/4 cases). In particular, CALMs and freckling were not observed. None of the four subjects was diagnosed with cancer.

RASopathy-causing *SPRED2* variants affect protein synthesis/stability, localization, and function

The homozygous occurrence of the three *SPRED2* variants in the four affected individuals and the predicted LoF

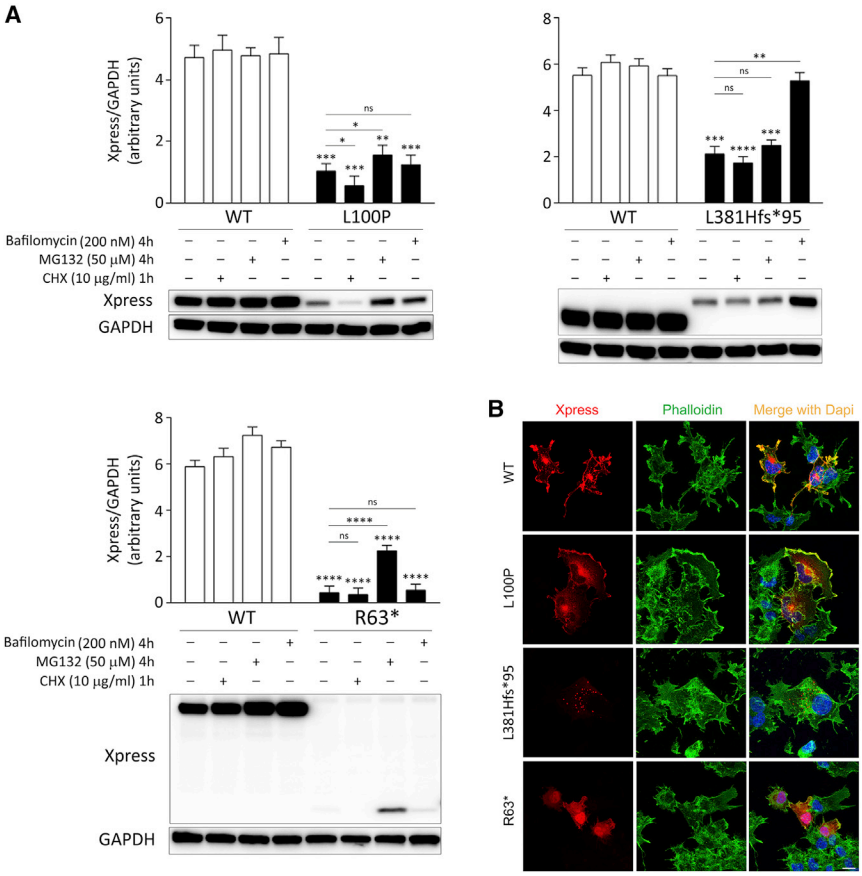

Figure 2. Biochemical characterization of the RASopathy-causing SPRED2 proteins

(A) Accelerated degradation of the SPRED2^{Arg63*} (R63*), SPRED2^{Leu100Pro} (L100P), and SPRED2^{Leu381Hisfs*95} (L381Hfs*95) proteins. WB analysis shows WT and variant Xpress-tagged SPRED2 protein levels in transfected COS-1 cells, basally and after CHX (10 μg/mL), MG132 (50 μM), or bafilomycin A1 (200 nM) treatment. As shown, accelerated degradation of SPRED2^{Arg63*} mainly occurs via the proteasome, while SPRED2^{Leu381Hisfs*95} is degraded primarily via autophagy/lysosomes. Both pathways are involved in the accelerated degradation of SPRED2^{Leu100Pro}, with a more relevant role of the proteasome (slight but statistically significant increased protein level in cells treated with MG132). GAPDH was used as loading control. Representative blots (below) and mean ± SD densitometry values (above) of three independent experiments are shown. Asterisks indicate statistically significant differences (*$p < 0.05$, **$p < 0.005$, ***$p < 0.001$, ****$p < 0.0001$, ns indicates not significant; two-way ANOVA followed by Sidak's multiple comparison test). (B) Subcellular localization of transiently expressed Xpress-tagged WT or mutated SPRED2 proteins in COS-1 cells under steady-state conditions revealed by confocal microscopy analysis. Cells were stained using an anti-Xpress monoclonal antibody and Alexa Fluor 594 goat anti-mouse secondary antibody (red). The F-actin dye Alexa Fluor 488 phalloidin (green) was used to stain the cortical actin associated with the plasma membrane. Merged images with nuclei (DAPI staining, blue) are displayed on the right panels. Scale bar, 10 μm.

impact for two of them supported a model in which disease-associated *SPRED2* variants have disruptive consequences on SPRED2 synthesis, stability, and/or function. According to a model recently developed to predict occurrence of nonsense-mediated mRNA decay (NMD) triggered by premature stop codons,[58] the c.187C>T change (subject 3-II-1) was expected to cause *SPRED2* mRNA degradation (NMD score > 0.6). Since biological material from subject 3-II-1 (or her parents) was not available to validate this prediction, we assume that NMD likely contributes to the LoF impact of the c.187C>T substitution, even though the synthesis of a residual truncated SPRED2 protein cannot be ruled out *a priori*. To validate the impact of the identified variants on SPRED2 stability, the three Xpress-tagged SPRED2 proteins were generated, and the protein level of each was assessed in transiently transfected COS-1 cells, basally and after 1 h treatment with the protein synthesis inhibitor CHX. Immunoblotting and relative quantitative analyses revealed a variably reduced level of the three proteins, indicating that the tested variants significantly impact SPRED2 stability (Figure 2A). As expected, the strongest effect was documented for the truncating variant at the N terminus. Treatment with MG132, an inhibitor of proteasomal activity, and bafilomycin, a late-stage inhibitor of autophagy and lysosomal protein degradation, variably rescued the reduced levels of SPRED2^{Arg63*} and SPRED2^{Leu381Hisfs*95}, respectively, indicating a different route of degradation for these proteins (Figure 2A). On the other hand, blocking either of the two pathways had little effect on the accelerated degradation of SPRED2^{Leu100Pro}, indicating that both routes actively contribute to the degradation of this variant, possibly with a more relevant role of the proteasome, as documented by the slight but statistically significant increased level of the protein in cells treated with MG132.

The negative modulatory role of SPRED proteins on RAS signaling requires their targeting to the plasma membrane, which is mediated by the SPR domain.[33] Indeed, SPRED variants lacking the SPR domain fail to translocate to the plasma membrane and downmodulate MAPK signaling.[36] By confocal laser scanning microscopy analysis of COS-1 cells transiently transfected to express an Xpress-tagged SPRED2, we confirmed the localization of the WT protein to the plasma membrane, as shown by

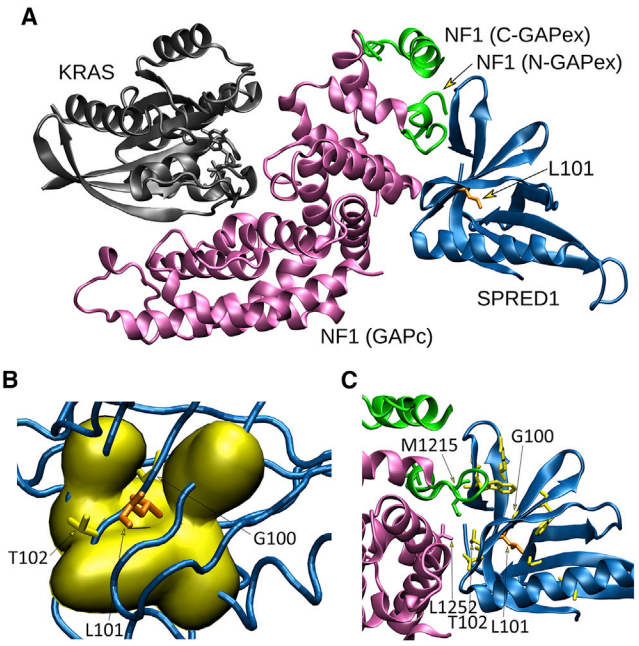

Figure 3. Structural impact of the p.Leu100Pro substitution in SPRED2

(A) The crystallographic complex of neurofibromin (NF1) GRD (GAPc, magenta) with the EVH1 domain of SPRED1 (blue) and GTP-bound KRAS (gray) is shown. The N- and C-terminal GAPex stretches encompassing GAPc are shown in green. The lateral chain of Leu^{101} (L101) (corresponding to Leu^{100} in SPRED2) is shown (orange).

(B) Surface visualization (Gaussian density surface) of the hydrophobic residues close to Leu^{101} (i.e., Ala^{19}, Val^{21}, Val^{42}, Trp^{92}, Phe^{103}, and Phe^{112}) is shown in yellow. Lateral chains of Leu^{101} and adjacent residues, Gly^{100} (G100) and Thr^{102} (T102), mutated in LGSS, are shown.

(C) Enlarged view of the neurofibromin and SPRED1 interacting surfaces. Relevant residues are indicated using the single-letter amino acid code. Lateral chains of SPRED1 residues (Arg^{24}, Gly^{30}, Trp^{31}, Val^{44}, Gly^{62}, Thr^{88}, Trp^{92}, Gly^{100}, and Thr^{102}) mutated in LGSS are shown (yellow), together with Leu^{101} (orange). Of note, Thr^{102} interacts with both GAPc (Leu^{1252}) and GAPex (Met^{1215}).

co-localization with cortical F-actin (Figure 2B). Assessment of the subcellular localization of the three SPRED2 variants documented that, similar to the WT protein, residual SPRED2^{Leu100Pro} showed, in part, proper targeting to the plasma membrane. In contrast, a diffuse localization in both cytoplasm and nucleus was documented for SPRED2^{Arg63*}, and a punctate localization pattern was observed for SPRED2^{Leu381Hisfs*95}, suggestive of vesicular distribution (Figure 2B). For the latter, treatment with bafilomycin resulted in an accumulation of puncta (Figure S5), which is in line with the preferential degradation of this variant via lysosomes.

Different from the other variants, the residual SPRED2^{Leu100Pro} protein retained a proper localization to the membrane, which is consistent with an unaffected SPR domain. Leu^{100} is located within the EVH1 domain, which is known to mediate protein-protein interactions. In SPRED1, this domain binds to the GRD of neurofibromin[33,34] and is required for the negative modulation of RAS function. The EVH1 of SPRED2 binds to neurofibromin with comparable affinity.[33,59] Remarkably, different LGSS-causing missense *SPRED1* changes affecting a residue adjacent to Leu^{100} in SPRED2 (Thr^{102}) and impairing binding to neurofibromin have been reported.[34,60] Based on these considerations, we hypothesized a perturbation of the ability of SPRED2^{Leu100Pro} to promote efficient translocation of neurofibromin to the plasma membrane as a contributing molecular mechanism underlying the functional dysregulation of this protein. To assess this hypothesis, we first explored the possible structural impact of the p.Leu100Pro substitution using the recently solved structure of the complex in which the neurofibromin GRD interacts with the EVH1 domain of SPRED1 and GTP-bound KRAS.[34] SPRED1 and SPRED2 EVH1 domains show a high homology in sequence and all residues flanking Leu^{100} (Leu^{101} in SPRED1) are conserved. A closer view into the complex revealed that Leu^{101} localized in a β sheet of the EVH1 domain mediating direct interaction with the neurofibromin GRD (Figure 3A). Its lateral chain is buried in the core of the domain and contributes to the intramolecular binding network stabilizing the region (Figure 3B). Specifically, Leu^{101} is at the center of a hydrophobic cluster formed by Ala^{19}, Val^{21}, Val^{42}, Trp^{92}, Phe^{103}, and Phe^{112}, which are all conserved in SPRED2. Leu^{101} forms a main chain hydrogen bond with His^{90}. The adjacent Thr^{102} (Thr^{101} in SPRED2) is an exposed residue with its lateral chain directly contributing to the intermolecular binding network with the neurofibromin GRD (Figure 3C).[34,60] The Leu-to-Pro substitution is expected to result in a substantial conformational rearrangement of this region and affect the ability of the EVH1 domain to efficiently bind to the GRD of neurofibromin. These considerations suggest that besides its impact on stability and the observed accelerated degradation, the p.Leu100Pro substitution likely results in a SPRED2 protein with decreased and/or less stable binding to neurofibromin, which is in line with previously published data documenting a similar behavior of SPRED1 variants causing LGSS.[34,59,60] To validate this hypothesis we evaluated the ability of SPRED2^{Leu100Pro} to bind to neurofibromin. First, we transfected COS-1 cells with V5-tagged neurofibromin GRD alone or with Xpress-tagged WT or variant *SPRED2* constructs. Following starvation and EGF stimulation, subcellular localization of SPRED2 proteins and neurofibromin GRD was analyzed by confocal microscopy. Expressed alone, neurofibromin GRD localized primarily in the cytoplasm (data not shown). When co-expressed, co-localization of WT SPRED2 and neurofibromin GRD at the plasma membrane was observed, indicating that SPRED2 facilitates plasma membrane translocation of the domain (Figure 4A). In contrast, GRD-SPRED2^{Leu100Pro} co-localization at the plasma membrane was not observed in cells overexpressing the SPRED2 variant, indicating that this protein fails to recruit neurofibromin GRD to the plasma membrane. To confirm the defective interaction

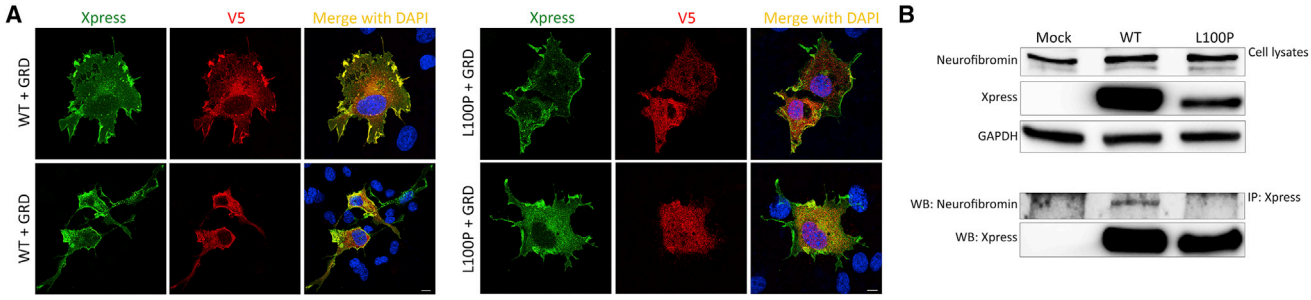

Figure 4. p.Leu100Pro results in a defective SPRED2 binding to neurofibromin
(A) Subcellular localization of transiently expressed V5-tagged GRD and Xpress-tagged WT or SPRED2^{Leu100Pro} (L100P) proteins in COS-1 cells after stimulation with EGF (30 ng/mL, 5 min) revealed by confocal microscopy analysis. Cells were stained using anti-Xpress IgG1 and anti-V5 IgG2a monoclonal antibodies and revealed by goat anti-mouse IgG1 Alexa Fluor 647 (pseudocolored in green) and goat anti-mouse IgG2a Alexa Fluor 594 (red) secondary antibodies, respectively. Nuclei are visualized by DAPI staining (blue). Scale bar, 10 μm. (B) Co-immunoprecipitation assays. Lysates from HEK293T cells transiently transfected to express WT or variant Xpress-tagged SPRED2 protein were serum-starved, stimulated with EGF (30 ng/mL), and immunoprecipitated with an anti-Xpress antibody and assayed by western blotting using the indicated antibodies.

of SPRED2^{Leu100Pro} with neurofibromin, we performed co-immunoprecipitation assays in cells overexpressing the WT and variant *SPRED2* constructs in HEK293T cells, starved and stimulated with EGF. As expected, endogenous neurofibromin co-immunoprecipitated with the WT SPRED2 protein but did not with SPRED2^{Leu100Pro} (Figure 4B). Overall, the *in silico* and *in vitro* data consistently indicate that the residual SPRED2^{Leu100Pro} protein is able to translocate to the plasma membrane but has a defective ability to mediate neurofibromin localization at the plasma membrane.

RASopathy-causing *SPRED2* variants fail to downmodulate MAPK signaling

SPRED2-decreased stability, impaired plasma membrane localization, and defective neurofibromin binding are expected to converge toward a flawed downmodulation of RAS-MAPK signaling. We explored the consequences of the identified *SPRED2* variants on this pathway by transiently transfecting each NS-associated SPRED2 protein in HEK293T cells and assessing the phosphorylation levels of the three tiers of the MAPK cascade, under basal conditions and following EGF stimulation, in time-course experiments (Figure 5A). None of the overexpressed SPRED2 variants promoted a significant perturbation of the dynamics and strength of RAF1, MEK, and ERK phosphorylation, while expression of the WT protein was associated with a slight but significant downmodulation of signaling when compared to control cells (mock transfection). Primary fibroblasts obtained from skin biopsies from subjects 1-II-1 (p.Leu381Hisfs*95) and 2-II-1 (p.Leu100Pro) were used in time-course experiments to assess the MAPK pathway activation in response to EGF stimulation. These assays confirmed a variably enhanced RAF1, MEK, and ERK phosphorylation in cells with bi-allelic *SPRED2* variants compared to control cells (Figure 5B), indicating MAPK signaling upregulation. Notably, in both fibroblast lines, signaling was not constitutively activated, retaining dependence on EGF stimulation. These findings confirmed that the bi-allelic *SPRED2* variants result in inactive proteins unable to efficiently downmodulate signal flow through the RAS-MAPK cascade, and that primary fibroblasts of subjects with impaired SPRED2 function show enhanced stimulus-dependent activation of this pathway.

In RASopathies, depending on the implicated gene/variant, dysregulated signal flow through the MAPK and/or phosphatidylinositol-3 kinase (PI3K)-AKT cascades is observed.[61–63] Consistent with previous data indicating that SPRED proteins do not participate in the control of PI3K-AKT signaling, no significant difference in the extent of EGF-stimulated AKT phosphorylation was documented by time-course experiments performed in primary fibroblasts from subjects 1-II-1 and 2-II-1 (Figure S6), confirming a specific functional link between SPRED2 and the MAPK cascade, at least in the present experimental conditions.

To validate the consequences of SPRED2 LoF in developmental processes reliant on MAPK signaling, we employed a MO-mediated *spred2* knockdown approach in zebrafish embryos to assess any perturbation of convergence and extension movements during gastrulation, a well-established readout of upregulated RAS-MAPK signaling that can be quantitatively evaluated by determining the major-to-minor axis ratio of embryos.[64–66] We first confirmed that the two annotated zebrafish *spred2a* and *spred2b* genes are homologous to human *SPRED2* by sequence alignment and phylogenetic analysis (Figure S7A) and documented that both genes are expressed during zebrafish embryogenesis, including early stages of development (Figure S7B). ATG-targeting MOs for both paralogs (Figure S1) were co-injected in embryos deriving from opportunely selected zebrafish pairs (Figure S1). *spred2a* and *spred2b* gene silencing was associated with increased Erk phosphorylation levels (Figure S8) and resulted in a high incidence of embryos showing delayed gastrulation, which arrested between 60% and 90% of epiboly (classified as "severe"), or delay in elongation during the segmentation stage, with reduced formation of the head and tailbud (classified as

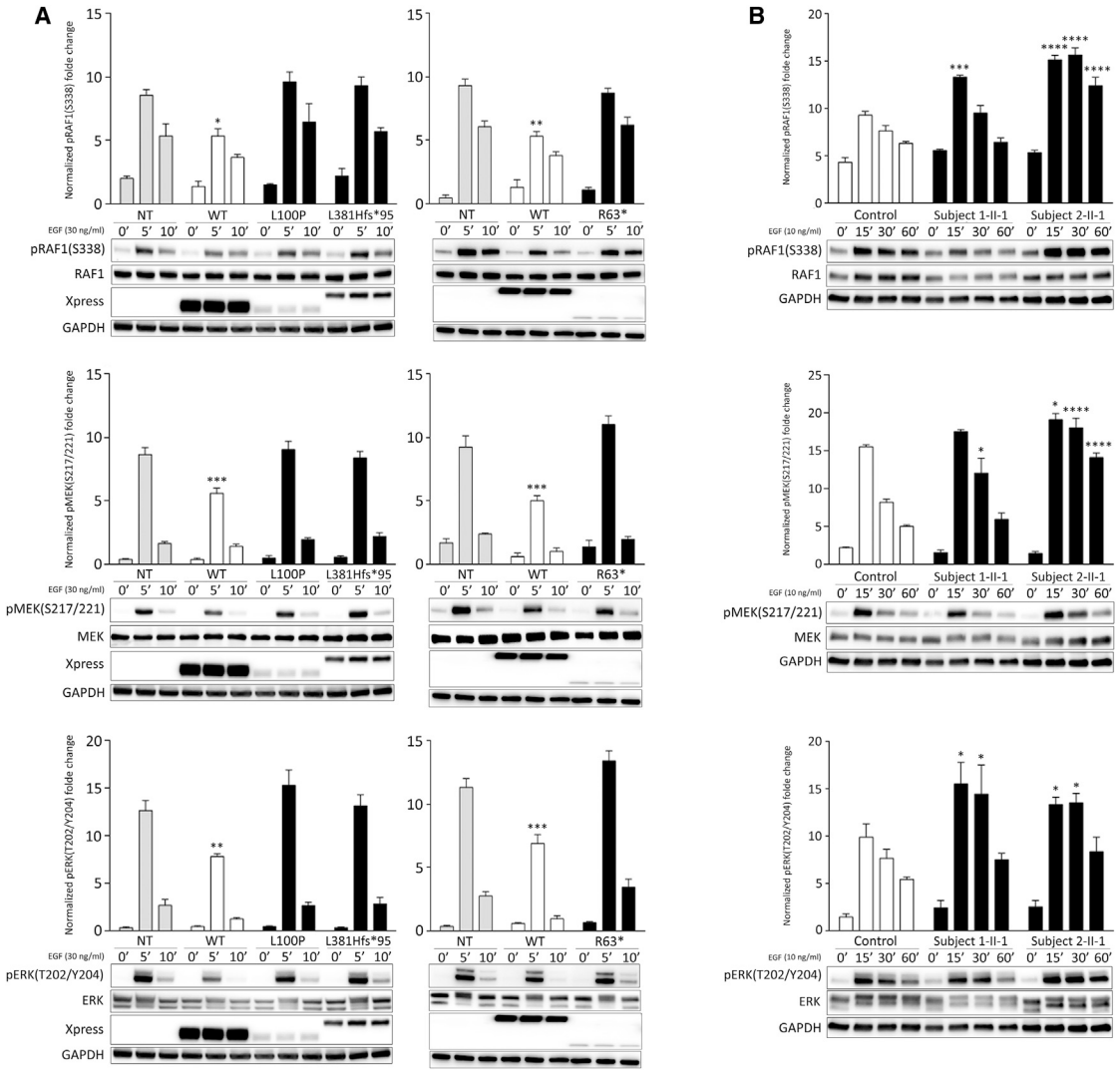

Figure 5. Impact of *SPRED2* mutations on MAPK signaling

(A) Overexpression of the RASopathy-causing SPRED2^{Arg63*} (R63*), SPRED2^{Leu100Pro} (L100P), and SPRED2^{Leu381Hisfs*95} (L381Hfs*95) proteins in HEK293T cells do not significantly perturb RAF1, MEK, and ERK phosphorylation as assessed by time-course experiments. Of note, expression of WT SPRED2 down-modulates ERK phosphorylation. HEK293T cells were transiently transfected with the indicated Xpress-tagged *SPRED2* constructs, serum-starved and treated with 30 ng/mL EGF for 5 or 10 min, or left unstimulated. Equal amounts of cell lysates were resolved on 10% polyacrylamide gel. Representative blots (below) and mean ± SD densitometry values (above) of three independent experiments are shown. Asterisks indicate statistically significant differences compared with control cells (NT, mock transfection) at the corresponding time upon EGF stimulation (*$p < 0.05$; **$p < 0.005$; ***$p < 0.001$; two-way ANOVA followed by Tukey's multiple comparison test).

(B) Primary fibroblasts from subjects 1-II-1 (p.Leu381Hisfs*95) and 2-II-1 (p.Leu100Pro) show variably enhanced RAF1, MEK, and ERK phosphorylation levels compared to control cells. Fibroblasts were starved for 16 h and then stimulated with EGF (10 ng/mL), in time-course experiments, or left unstimulated. Equal amounts of cell lysates were resolved on 10% polyacrylamide gel. Representative blots (below) and graphs reporting mean ± SD densitometry values (above) of three independent experiments are shown. Asterisks indicate statistically significant differences in the phosphorylation levels compared to control cells at the corresponding experimental points (*$p < 0.05$; ***$p < 0.001$; ****$p < 0.0001$; two-way ANOVA followed by Tukey's multiple comparison test).

"mild") (Figure 6A). The severe phenotype was rescued, in part, by concomitant microinjection of WT *SPRED2* mRNA, with a negligible effect of *SPRED2*^{Leu381Hisfs*95} (Figure 6B). Assessment of the major-to-minor axis ratio at 12 hpf documented a slight but statistically significant yolk elongation in *spred2* morphants, indicating enhanced MAPK signaling. Again, measuring the ratio in embryos co-injected with WT *SPRED2* mRNA documented a rescue of the phenotype (Figure 6C). However, no rescue of the phenotype was observed in embryos co-injected with an equal amount of *SPRED2*^{Leu381Hisfs*95} cDNA, confirming the LoF impact of the variant.

Spred2 KO mouse phenotyping

The previously generated *Spred2*$^{-/-}$ mouse model was phenotypically inspected to investigate the occurrence of the features and signs characterizing the subjects with bi-allelic inactivating *SPRED2* variants.[54] Compared to their

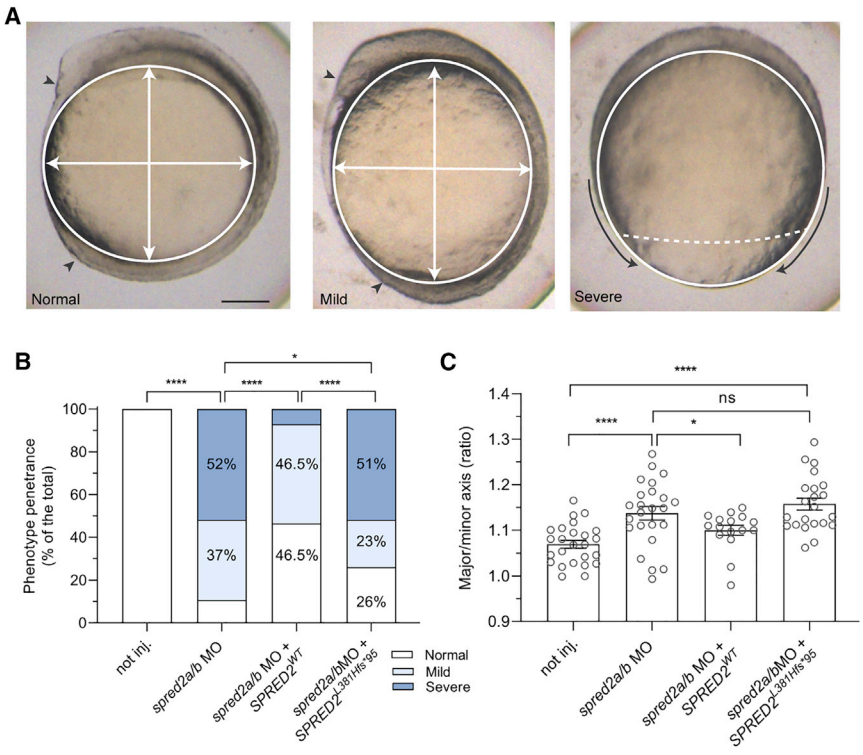

Figure 6. Consequences of MO-mediated *Spred2* silencing on early zebrafish embryonic development

(A) Phenotype classification (normal, mild, and severe) and quantification in embryos at around 11–12 hpf injected with antisense oligonucleotides (MO) (6 ng) against *spred2a* and *spred2b* with or without mRNA encoding WT SPRED2 (1.5 pg). Representative pictures for the different phenotypic classes are shown in the upper panel. Arrowheads indicate the head and tailbuds, black arrows show defective epiboly movements, white arrows indicate the major and minor axes. Scale bar: 125 μm.

(B) Overall number of embryos (%) exhibiting the different phenotypes (not injected, n = 24; MO, n = 19; MO + WT SPRED2, n = 19; MO + SPRED2^{Leu381Hisfs*95} [SPRED2^{L381Hfs*95}], n = 27). Two-tailed Fisher exact test was used to compare the prevalence of "normal" and "severe" phenotypic classes (*p < 0.05, ****p < 0.0001).

(C) Quantification of the oval shape (major-to-minor axis ratio) (not injected, n = 25; MO, n = 26; MO + WT SPRED2, n = 16; MO + SPRED2^{Leu381Hisfs*95} [SPRED2^{L381Hfs*95}], n = 22). Mean ± SEM is shown and one-way ANOVA with two-stage Benjamini, Krieger, and Yekutieli procedure was used for statistical assessment (*p < 0.05, ****p < 0.0001).

age-matched and gender-matched *Spred2*$^{+/+}$ littermates, *Spred2*$^{-/-}$ mice regularly developed kyphosis and scoliosis (Figures 7A and 7B). The skeletal defects were accompanied by growth retardation, as previously reported (Figure 7C).[54] Of note, altered craniofacial development was also appreciated (Figure 7D). Specifically, mice showed a dome-shaped forehead and a shortened nose. Quantification of skull length in X-ray images revealed a gender-independent reduction of skull length in *Spred2*$^{-/-}$ mice (Figure 7E). These craniofacial features were often associated with a misalignment of the incisors (Figure 7F). Increasing with age, *Spred2*$^{-/-}$ mice developed splenomegaly (extreme example in Figure 7G), as documented by the increased spleen to body weight ratio (Figure 7H). Suggestive of cardiac hypertrophy, assessment of heart weight revealed a gender-independent increase of heart weight to body weight ratio in KO mice (Figure 7I), in line with the previously reported hypertrophic state of cardiomyocytes.[67] In addition, consistent with previous observations,[67] various ventricular cardiac arrhythmias were recorded in *Spred2*$^{-/-}$ mice (Figure 7J), as well supraventricular arrhythmias (Figure 7K). Notably, *Spred2*$^{-/-}$ mice showed an elevated volume of the ventricular system of the brain (Figure S9), and the dentate gyrus region of the hippocampus appeared not fully developed, which was accompanied by an enhanced Ras activity in this region (Figure S10). Furthermore, with low penetrance, mice developed dilated Bowman's capsules, polycystic kidneys, and unilateral hydronephrosis (Figure S11). On the whole, the collected data indicated that *Spred2*$^{-/-}$ mice have craniofacial defects, reduced body size, splenomegaly, and cardiac hypertrophy with arrhythmias, similar to what is observed in the human disorder.

Discussion

Our findings provide evidence that loss of SPRED2 function underlies a recessive developmental disorder within the RASopathy clinical spectrum resembling NS. Complementary *in silico*, *in vitro*, and *in vivo* analyses documented that pathogenic *SPRED2* variants can affect protein stability, causing accelerated degradation, but can also affect proper targeting of SPRED2 to the plasma membrane or impair its binding to neurofibromin. These effects converge toward an upregulation of MAPK signaling. Remarkably, the associated clinical features significantly differ from those resulting from *SPRED1* haploinsufficiency occurring in LGSS.

SPRED2 is a member of a family of proteins functioning as negative regulators of signaling elicited by cell-surface receptor tyrosine kinases. Among these, four paralogs of the Sprouty subfamily (SPRY1-4) have been identified in mammals and documented to suppress the activation of the MAPK cascade induced in response to a variety of growth factors.[68] Their negative modulatory function is exerted at the level of RAS activation by preventing SOS translocation to membranes and its positive modulatory role on RAS function.[69] A negative regulatory role of these proteins on MAPK signaling by binding and inactivating RAF has also

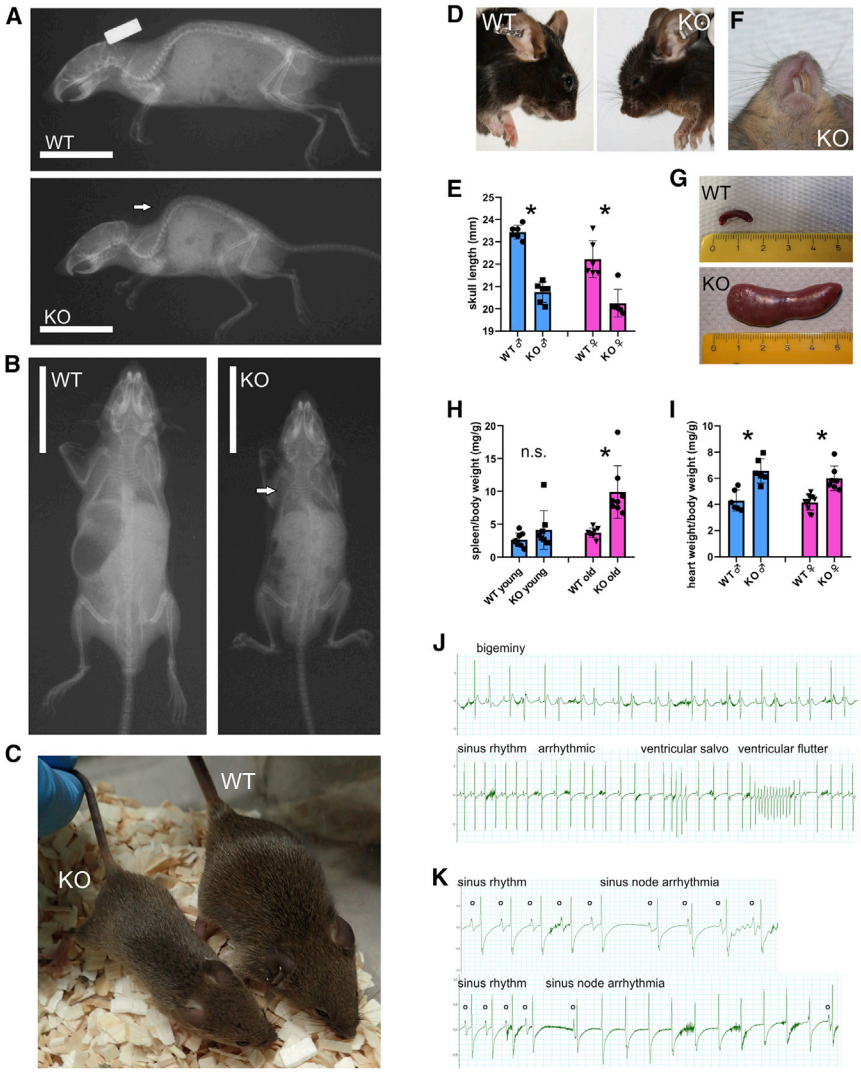

Figure 7. Phenotypic assessment of *Spred2* KO mice

(A) Soft X-ray images showing skeletal abnormalities in a *Spred2*$^{-/-}$ (KO) mouse compared to an age-matched WT littermate. Arrow labels kyphosis.

(B) X-ray images documenting scoliosis (arrow) in a KO mouse compared to an age-matched WT littermate.

(C) Representative photograph of male littermates at the age of 6 weeks showing growth retardation of a KO mouse (left) compared to an age-matched control animal (right).

(D) Comparison of the head shape of male littermates at the age of 6 months.

(E) Quantification of skull lengths taken from X-ray images (n = 6, each group; *p < 0.05).

(F) Representative photograph showing misaligned incisors in KO mice.

(G) Examples of spleens of mice at the age of 12 months showing a dramatic increase in spleen size of a KO mouse.

(H) Quantification of spleen to body weight ratios in young (6–8 weeks) and old (12 months) mice (n = 8 in each group; *p < 0.05).

(I) Comparison of heart weight to body weight ratios (n = 6 mice in each group; *p < 0.05).

(J) Examples of ventricular arrhythmias in KO mice at the age of 12 months.

(K) Examples of supraventricular arrhythmias in KO mice at the age of 12 months.

been suggested.[70] On the other hand, the three members of the SPRED subfamily negatively control MAPK signaling by promoting binding of neurofibromin to activated, GTP-bound RAS.[25] Among these, SPRED3 appears to have a lower inhibitory activity,[39] possibly as a result of a reduced affinity in neurofibromin binding.[59] Similarly, wide and partially overlapping expression patterns have been reported for *SPRED1* and *SPRED2* (Genotype-Tissue Expression Project [GTEx] portal, Human Protein Atlas), with the former being more broadly expressed during embryogenesis[71] and the latter more extensively expressed in adult organs and tissues.[35] In contrast, *Spred3* expression appears more restricted, being limited to the brain (GTEx portal).[39] These observations suggest a differential role of the three proteins in controlling MAPK signaling, which is in line with the different phenotypes characterizing the generated KO mice. Indeed, *Spred1*$^{-/-}$ mice show a lower body weight, a shortened face, spatial learning and memory deficits, and eosinophilia,[72,73] while *Spred2*$^{-/-}$ mice were reported to have a markedly reduced growth and shorter long bones,[54] cardiac fibrosis and arrhythmias, and a shortened lifespan.[67] The different features previously documented in these models, together with those observed in the present study (see below), indicate a differential role of these proteins in controlling bone morphogenesis, hematopoiesis, cardiac function, and multiple cellular processes (present study),[25,35,68] even though the finding that *Spred1* and *Spred2* KO mice are viable while *Spred1/2* double KO mice are embryonic lethal supports partial redundancy in function.[40]

Similar to what is observed in affected individuals, *Spred2*$^{-/-}$ mice showed signs of cardiac arrhythmias and hypertrophy, reduced growth and weight, kyphosis, cranial anomalies, splenomegaly, and enlargement of the brain ventricle system. The observed shortened skull, the splenomegaly, and the cardiac hypertrophy in *Spred2*$^{-/-}$ mice resemble phenotypes of the *Raf1*^{L613V}, *Kras*^{V14I}, and *Ptpn11*$^{D61G/+}$ mouse models of NS.[74–76] However, neither the pulmonary valve stenosis documented in affected individuals was replicated in *Spred2*$^{-/-}$ mice, nor other changes in right ventricular hemodynamics were detected in mice. So far, malformation of the gyrus dentatus and kidney features were detected only in mice, possibly due to the small number of identified subjects with bi-allelic inactivating *SPRED2* variants or/and young age of the affected subjects.

The obsessive-compulsive disorder-like behavior observed in *Spred2*$^{-/-}$ mice is supportive for potential behavioral changes in affected individuals;[77] on the other hand, no data are currently available concerning cognitive or learning aspects in these mice.

Among the members of the SPRY/SPRED family, only *SPRED1* had previously been established to be implicated in a Mendelian disorder,[13] while heterozygous missense variants of *SPRY4* (MIM: 607984) had been reported as a contributing event in congenital hypogonadotropic hypogonadism (MIM: 615266), a condition characterized by oligogenic inheritance.[78] Here, we report that *SPRED2* is also causally associated with a Mendelian disorder. The four affected individuals from the three unrelated consanguineous families here reported were identified in the frame of a multicentric collaborative effort (NSEuroNet consortium). Two unrelated individuals were identified at the University Hospital of Magdeburg among 320 subjects with a tentative diagnosis of RASopathy found negative for mutations in previously known genes. One individual (3-II-1) was identified among 1,664 affected individuals screened at the Robert Debré Hospital, Paris, for diagnostic testing for NS or a related disorder. Finally, no bi-allelic occurrence of functionally relevant *SPRED2* variants was identified among 40 subjects with a suspected clinical diagnosis of RASopathy, negative for pathogenic variants in known genes implicated in these disorders, who were assessed by exome sequencing (Ospedale Pediatrico Bambino Gesù, Rome) and among 471 affected individuals referred for genetic testing because of a suspected RASopathy screened at the Policlinico S. Orsola, Bologna, and Fondazione Casa Sollievo della Sofferenza, San Giovanni Rotondo (among these 57/471 were positive for pathogenic *PTPN11* variants). Overall, these findings indicate that mutations in *SPRED2* likely account for a relatively small proportion of affected individuals with clinical diagnosis suggestive of NS and are very uncommon in a non-consanguineous setting, though structural rearrangements (e.g., large intragenic deletions) and variants affecting regulatory and deep intronic regions were not systematically considered in our mutational scanning effort.

In contrast with the significant overlap between LGSS and NF1, the clinical features occurring in the identified subjects with bi-allelic inactivating *SPRED2* variants are more closely related to NS (Table S1). LGSS, which is caused by heterozygous inactivating variants in *SPRED1*, is a substantially mild version of NF1.[31] In LGSS, multiple CALMs freckling, DD, learning difficulties, and behavioral problems commonly occur. NS-like craniofacial features are also a relatively common finding, while Lisch nodules, neurofibromas, optic gliomas, malignant peripheral nerve sheath tumors, and NF1-specific bone lesions are essentially absent. Different from what is observed in LGSS, the phenotypes associated with disrupted SPRED2 function fit well within the clinical spectrum of NS, with short stature, a short/webbed neck with a low posterior hairline, ID, and craniofacial and thorax features resembling NS. Cardiac involvement (CHD and HCM), which is generally not observed in LGSS and is a recurrent feature of NS, was reported in three of the four subjects, and included ECG anomalies, HCM, and PVS. Of note, CALMs or axillary/inguinal freckling were not reported in these subjects. Moreover, differently from LGSS, the present condition is inherited as a recessive trait, which further supports partial redundancy. The distinct clinical presentations associated with *SPRED1* haploinsufficiency and SPRED2 LoF support the idea that these proteins play different roles in development. While dedicated studies are required to dissect the role of these proteins in the modulation of RAS-MAPK signaling, multiple factors likely contribute to this picture. On one hand, the two genes are characterized by only partially overlapping expression patterns in adult tissues and during development, which are expected to contribute to the "unique" ability of the two proteins to control the amplitude and duration of activation of the MAPK cascade in response of various extracellular signals and in a specific temporal and spatial manner. On the other hand, it is also likely that the two proteins have different strengths in contributing to the tuning mechanism regulating the intensity and dynamics of MAPK signaling, and that the cellular context might be relevant for such function. Overall, both quantitative and qualitative aspects likely are relevant in explaining the diverse phenotype associated with decreased/loss of function of SPRED1 and SPRED2. While dedicated efforts are required to answer these questions, a noticeable finding of this study is the occurrence of conserved themes in the functional dysregulation associated with pathogenic *SPRED1* and *SPRED2* variants. Previous functional characterization of the molecular causes leading to *SPRED1* haploinsufficiency in LGSS documented various aspects of the biochemical behavior, including defective protein synthesis or accelerated degradation, aberrant localization, and impaired interaction with neurofibromin, as the invariantly occurring events.[32,34,59] The same key aspects were found to be affected by the bi-allelic *SPRED2* variants implicated in the present recessive NS-like disorder.

To conclude, we provide evidence that inactivating bi-allelic variants in *SPRED2* underlie a rare recessive clinical phenotype that is distinct from LGSS and resembles NS. These pathogenic variants affect different properties of the protein but are functionally equivalent, causing loss of SPRED2 function and upregulation of MAPK signaling. Further studies are required to more accurately understand the different modulatory function of SPRED proteins in intracellular signaling and development.

Data and code availability

The pathogenic variants identified in this work have been submitted to ClinVar with accession numbers: c.187C>T (p.Arg63*), SCV001809842; c.299T>C (p.Leu100Pro), SCV001805865; and c.1142_1143delTT (p.Leu381Hisfs*95), SCV001805864.

Supplemental information

Supplemental information can be found online at https://doi.org/10.1016/j.ajhg.2021.09.007.

Acknowledgments

The authors thank the subjects and their families for participating in this study. This work was supported by grants from EJP-RD (NSEuroNet, to H.C., M.Z. [FZK 01GM1921A], and M.T.), AIRC (IG 21614 to M.T.), Ministero della Salute (Ricerca Corrente 2020 and 2021 to A.D.L. and M.T.; CCR-2017-23669081 and RCR-2020-23670068_001 to M.T.; RF-2018-12366931 to F.C.R., G.C., and B.D.), Ministero della Ricerca (FOE 2019 to M.T.), German Research Foundation (SCHU1600/6-1 to K.S.), and German Federal Ministry of Education and Research - BMBF (German Network for RASopathy Research "GeNeRARe" [FKZ: 01GM1902A]) to M.Z. This work has been carried out in the frame of the European Reference Network on Rare Congenital Malformations and Rare Intellectual Disability (ERN-ITHACA) activity.

Declaration of interests

The authors declare no competing interests.

Received: July 21, 2021
Accepted: September 14, 2021
Published: October 8, 2021

Web resources

CADD, https://cadd.gs.washington.edu/
ClinVar, https://www.ncbi.nlm.nih.gov/clinvar/
COSMIC, https://cancer.sanger.ac.uk/cosmic
dbSNP, https://www.ncbi.nlm.nih.gov/projects/SNP/
ExAC Browser, http://exac.broadinstitute.org/
GenBank, https://www.ncbi.nlm.nih.gov/genbank/
gnomAD Browser, https://gnomad.broadinstitute.org/
GTEx Portal, https://gtexportal.org/home/
MetaDome, https://stuart.radboudumc.nl/metadome/
MUSCLE, https://www.ebi.ac.uk/Tools/msa/muscle/
OMIM, https://www.omim.org/
PhyML, http://www.atgc-montpellier.fr/phyml/
pyBoxshade, https://github.com/mdbaron42/pyBoxshade
RCSB Protein Data Bank, http://www.rcsb.org/pdb/home/home.do
SWISS-MODEL, https://swissmodel.expasy.org/
The Human Protein Atlas, http://www.proteinatlas.org/

References

1. Yoon, S., and Seger, R. (2006). The extracellular signal-regulated kinase: multiple substrates regulate diverse cellular functions. Growth Factors *24*, 21–44.
2. Castellano, E., and Santos, E. (2011). Functional specificity of ras isoforms: so similar but so different. Genes Cancer *2*, 216–231.
3. Johnson, L., Greenbaum, D., Cichowski, K., Mercer, K., Murphy, E., Schmitt, E., Bronson, R.T., Umanoff, H., Edelmann, W., Kucherlapati, R., and Jacks, T. (1997). K-ras is an essential gene in the mouse with partial functional overlap with N-ras. Genes Dev. *11*, 2468–2481.
4. Krens, S.F., Spaink, H.P., and Snaar-Jagalska, B.E. (2006). Functions of the MAPK family in vertebrate-development. FEBS Lett. *580*, 4984–4990.
5. Thomas, G.M., and Huganir, R.L. (2004). MAPK cascade signalling and synaptic plasticity. Nat. Rev. Neurosci. *5*, 173–183.
6. Fuentes-Mateos, R., Jimeno, D., Gómez, C., Calzada, N., Fernández-Medarde, A., and Santos, E. (2019). Concomitant deletion of HRAS and NRAS leads to pulmonary immaturity, respiratory failure and neonatal death in mice. Cell Death Dis. *10*, 838.
7. Hayashi, S., and Ogura, Y. (2020). ERK signaling dynamics in the morphogenesis and homeostasis of Drosophila. Curr. Opin. Genet. Dev. *63*, 9–15.
8. Tartaglia, M., and Gelb, B.D. (2010). Disorders of dysregulated signal traffic through the RAS-MAPK pathway: phenotypic spectrum and molecular mechanisms. Ann. N Y Acad. Sci. *1214*, 99–121.
9. Pylayeva-Gupta, Y., Grabocka, E., and Bar-Sagi, D. (2011). RAS oncogenes: weaving a tumorigenic web. Nat. Rev. Cancer *11*, 761–774.
10. Rauen, K.A. (2013). The RASopathies. Annu. Rev. Genomics Hum. Genet. *14*, 355–369.
11. Simanshu, D.K., Nissley, D.V., and McCormick, F. (2017). RAS proteins and their regulators in human disease. Cell *170*, 17–33.
12. Upadhyaya, M., Shen, M., Cherryson, A., Farnham, J., Maynard, J., Huson, S.M., and Harper, P.S. (1992). Analysis of mutations at the neurofibromatosis 1 (NF1) locus. Hum. Mol. Genet. *1*, 735–740.
13. Brems, H., Chmara, M., Sahbatou, M., Denayer, E., Taniguchi, K., Kato, R., Somers, R., Messiaen, L., De Schepper, S., Fryns, J.P., et al. (2007). Germline loss-of-function mutations in SPRED1 cause a neurofibromatosis 1-like phenotype. Nat. Genet. *39*, 1120–1126.
14. Martinelli, S., De Luca, A., Stellacci, E., Rossi, C., Checquolo, S., Lepri, F., Caputo, V., Silvano, M., Buscherini, F., Consoli, F., et al. (2010). Heterozygous germline mutations in the CBL tumor-suppressor gene cause a Noonan syndrome-like phenotype. Am. J. Hum. Genet. *87*, 250–257.
15. Yamamoto, G.L., Aguena, M., Gos, M., Hung, C., Pilch, J., Fahiminiya, S., Abramowicz, A., Cristian, I., Buscarilli, M., Naslavsky, M.S., et al. (2015). Rare variants in SOS2 and LZTR1 are associated with Noonan syndrome. J. Med. Genet. *52*, 413–421.
16. Aoki, Y., Niihori, T., Inoue, S., and Matsubara, Y. (2016). Recent advances in RASopathies. J. Hum. Genet. *61*, 33–39.
17. Tajan, M., Paccoud, R., Branka, S., Edouard, T., and Yart, A. (2018). The RASopathy family: consequences of germline activation of the RAS/MAPK pathway. Endocr. Rev. *39*, 676–700.
18. Johnston, J.J., van der Smagt, J.J., Rosenfeld, J.A., Pagnamenta, A.T., Alswaid, A., Baker, E.H., Blair, E., Borck, G., Brinkmann, J., Craigen, W., et al.; Members of the Undiagnosed Diseases Network (2018). Autosomal recessive Noonan syndrome associated with biallelic LZTR1 variants. Genet. Med. *20*, 1175–1185.
19. Pagnamenta, A.T., Kaisaki, P.J., Bennett, F., Burkitt-Wright, E., Martin, H.C., Ferla, M.P., Taylor, J.M., Gompertz, L., Lahiri, N., Tatton-Brown, K., et al.; DDD Study (2019). Delineation of dominant and recessive forms of LZTR1-associated Noonan syndrome. Clin. Genet. *95*, 693–703.

20. Maher, G.J., Ralph, H.K., Ding, Z., Koelling, N., Mlcochova, H., Giannoulatou, E., Dhami, P., Paul, D.S., Stricker, S.H., Beck, S., et al. (2018). Selfish mutations dysregulating RAS-MAPK signaling are pervasive in aged human testes. Genome Res. *28*, 1779–1790.
21. Grant, A.R., Cushman, B.J., Cavé, H., Dillon, M.W., Gelb, B.D., Gripp, K.W., Lee, J.A., Mason-Suares, H., Rauen, K.A., Tartaglia, M., et al. (2018). Assessing the gene-disease association of 19 genes with the RASopathies using the ClinGen gene curation framework. Hum. Mutat. *39*, 1485–1493.
22. Niihori, T., Nagai, K., Fujita, A., Ohashi, H., Okamoto, N., Okada, S., Harada, A., Kihara, H., Arbogast, T., Funayama, R., et al. (2019). Germline-Activating RRAS2 Mutations Cause Noonan Syndrome. Am. J. Hum. Genet. *104*, 1233–1240.
23. Capri, Y., Flex, E., Krumbach, O.H.F., Carpentieri, G., Cecchetti, S., Lißewski, C., Rezaei Adariani, S., Schanze, D., Brinkmann, J., Piard, J., et al. (2019). Activating Mutations of RRAS2 Are a Rare Cause of Noonan Syndrome. Am. J. Hum. Genet. *104*, 1223–1232.
24. Motta, M., Pannone, L., Pantaleoni, F., Bocchinfuso, G., Radio, F.C., Cecchetti, S., Ciolfi, A., Di Rocco, M., Elting, M.W., Brilstra, E.H., et al. (2020). Enhanced MAPK1 Function Causes a Neurodevelopmental Disorder within the RASopathy Clinical Spectrum. Am. J. Hum. Genet. *107*, 499–513.
25. Lorenzo, C., and McCormick, F. (2020). SPRED proteins and their roles in signal transduction, development, and malignancy. Genes Dev. *34*, 1410–1421.
26. Legius, E., Messiaen, L., Wolkenstein, P., Pancza, P., Avery, R.A., Berman, Y., Blakeley, J., Babovic-Vuksanovic, D., Cunha, K.S., Ferner, R., et al.; International Consensus Group on Neurofibromatosis Diagnostic Criteria (I-NF-DC) (2021). Revised diagnostic criteria for neurofibromatosis type 1 and Legius syndrome: an international consensus recommendation. Genet. Med. *23*, 1506–1513.
27. Scheffzek, K., Ahmadian, M.R., Wiesmüller, L., Kabsch, W., Stege, P., Schmitz, F., and Wittinghofer, A. (1998). Structural analysis of the GAP-related domain from neurofibromin and its implications. EMBO J. *17*, 4313–4327.
28. Bos, J.L., Rehmann, H., and Wittinghofer, A. (2007). GEFs and GAPs: critical elements in the control of small G proteins. Cell *129*, 865–877.
29. De Luca, A., Bottillo, I., Sarkozy, A., Carta, C., Neri, C., Bellacchio, E., Schirinzi, A., Conti, E., Zampino, G., Battaglia, A., et al. (2005). NF1 gene mutations represent the major molecular event underlying neurofibromatosis-Noonan syndrome. Am. J. Hum. Genet. *77*, 1092–1101.
30. Pinna, V., Lanari, V., Daniele, P., Consoli, F., Agolini, E., Margiotti, K., Bottillo, I., Torrente, I., Bruselles, A., Fusilli, C., et al. (2015). p.Arg1809Cys substitution in neurofibromin is associated with a distinctive NF1 phenotype without neurofibromas. Eur. J. Hum. Genet. *23*, 1068–1071.
31. Brems, H., and Legius, E. (2013). Legius syndrome, an Update. Molecular pathology of mutations in SPRED1. Keio J. Med. *62*, 107–112.
32. Brems, H., Pasmant, E., Van Minkelen, R., Wimmer, K., Upadhyaya, M., Legius, E., and Messiaen, L. (2012). Review and update of SPRED1 mutations causing Legius syndrome. Hum. Mutat. *33*, 1538–1546.
33. Stowe, I.B., Mercado, E.L., Stowe, T.R., Bell, E.L., Oses-Prieto, J.A., Hernández, H., Burlingame, A.L., and McCormick, F. (2012). A shared molecular mechanism underlies the human rasopathies Legius syndrome and Neurofibromatosis-1. Genes Dev. *26*, 1421–1426.
34. Yan, W., Markegard, E., Dharmaiah, S., Urisman, A., Drew, M., Esposito, D., Scheffzek, K., Nissley, D.V., McCormick, F., and Simanshu, D.K. (2020). Structural Insights into the SPRED1-Neurofibromin-KRAS Complex and Disruption of SPRED1-Neurofibromin Interaction by Oncogenic EGFR. Cell Rep. *32*, 107909.
35. Bundschu, K., Walter, U., and Schuh, K. (2007). Getting a first clue about SPRED functions. BioEssays *29*, 897–907.
36. King, J.A., Straffon, A.F., D'Abaco, G.M., Poon, C.L., i, S.T., Smith, C.M., Buchert, M., Corcoran, N.M., Hall, N.E., Callus, B.A., et al. (2005). Distinct requirements for the Sprouty domain for functional activity of Spred proteins. Biochem. J. *388*, 445–454.
37. Wakioka, T., Sasaki, A., Kato, R., Shouda, T., Matsumoto, A., Miyoshi, K., Tsuneoka, M., Komiya, S., Baron, R., and Yoshimura, A. (2001). Spred is a Sprouty-related suppressor of Ras signalling. Nature *412*, 647–651.
38. Lim, J., Yusoff, P., Wong, E.S., Chandramouli, S., Lao, D.H., Fong, C.W., and Guy, G.R. (2002). The cysteine-rich sprouty translocation domain targets mitogen-activated protein kinase inhibitory proteins to phosphatidylinositol 4,5-bisphosphate in plasma membranes. Mol. Cell. Biol. *22*, 7953–7966.
39. Kato, R., Nonami, A., Taketomi, T., Wakioka, T., Kuroiwa, A., Matsuda, Y., and Yoshimura, A. (2003). Molecular cloning of mammalian Spred-3 which suppresses tyrosine kinase-mediated Erk activation. Biochem. Biophys. Res. Commun. *302*, 767–772.
40. Taniguchi, K., Kohno, R., Ayada, T., Kato, R., Ichiyama, K., Morisada, T., Oike, Y., Yonemitsu, Y., Maehara, Y., and Yoshimura, A. (2007). Spreds are essential for embryonic lymphangiogenesis by regulating vascular endothelial growth factor receptor 3 signaling. Mol. Cell. Biol. *27*, 4541–4550.
41. Radio, F.C., Pang, K., Ciolfi, A., Levy, M.A., Hernández-García, A., Pedace, L., Pantaleoni, F., Liu, Z., de Boer, E., Jackson, A., et al. (2021). SPEN haploinsufficiency causes a neurodevelopmental disorder overlapping proximal 1p36 deletion syndrome with an episignature of X chromosomes in females. Am. J. Hum. Genet. *108*, 502–516.
42. Lin, Y.C., Niceta, M., Muto, V., Vona, B., Pagnamenta, A.T., Maroofian, R., Beetz, C., van Duyvenvoorde, H., Dentici, M.L., Lauffer, P., et al.; Genomics England Research Consortium (2021). SCUBE3 loss-of-function causes a recognizable recessive developmental disorder due to defective bone morphogenetic protein signaling. Am. J. Hum. Genet. *108*, 115–133.
43. Waterhouse, A., Bertoni, M., Bienert, S., Studer, G., Tauriello, G., Gumienny, R., Heer, F.T., de Beer, T.A.P., Rempfer, C., Bordoli, L., et al. (2018). SWISS-MODEL: homology modelling of protein structures and complexes. Nucleic Acids Res. *46* (W1), W296–W303.
44. Humphrey, W., Dalke, A., and Schulten, K. (1996). VMD: visual molecular dynamics. J. Mol. Graph. *14*, 33–38, 27–28.
45. Pettersen, E.F., Goddard, T.D., Huang, C.C., Couch, G.S., Greenblatt, D.M., Meng, E.C., and Ferrin, T.E. (2004). UCSF Chimera–a visualization system for exploratory research and analysis. J. Comput. Chem. *25*, 1605–1612.
46. Dunbrack, R.L.J., Jr. (2002). Rotamer libraries in the 21st century. Curr. Opin. Struct. Biol. *12*, 431–440.
47. Motta, M., Chillemi, G., Fodale, V., Cecchetti, S., Coppola, S., Stipo, S., Cordeddu, V., Macioce, P., Gelb, B.D., and Tartaglia,

M. (2016). SHOC2 subcellular shuttling requires the KEKE motif-rich region and N-terminal leucine-rich repeat domain and impacts on ERK signalling. Hum. Mol. Genet. *25*, 3824–3835.

48. Smith, P.K., Krohn, R.I., Hermanson, G.T., Mallia, A.K., Gartner, F.H., Provenzano, M.D., Fujimoto, E.K., Goeke, N.M., Olson, B.J., and Klenk, D.C. (1985). Measurement of protein using bicinchoninic acid. Anal. Biochem. *150*, 76–85.
49. Westerfield, M. (2000). The zebrafish book. A guide for the laboratory use of zebrafish (*Danio rerio*), Fourth Edition (Eugene: Univ. of Oregon Press).
50. LaFave, M.C., Varshney, G.K., Vemulapalli, M., Mullikin, J.C., and Burgess, S.M. (2014). A defined zebrafish line for high-throughput genetics and genomics: NHGRI-1. Genetics *198*, 167–170.
51. Bedell, V.M., Westcot, S.E., and Ekker, S.C. (2011). Lessons from morpholino-based screening in zebrafish. Brief. Funct. Genomics *10*, 181–188.
52. Robu, M.E., Larson, J.D., Nasevicius, A., Beiraghi, S., Brenner, C., Farber, S.A., and Ekker, S.C. (2007). p53 activation by knockdown technologies. PLoS Genet. *3*, e78.
53. Schindelin, J., Arganda-Carreras, I., Frise, E., Kaynig, V., Longair, M., Pietzsch, T., Preibisch, S., Rueden, C., Saalfeld, S., Schmid, B., et al. (2012). Fiji: an open-source platform for biological-image analysis. Nat. Methods *9*, 676–682.
54. Bundschu, K., Knobeloch, K.P., Ullrich, M., Schinke, T., Amling, M., Engelhardt, C.M., Renné, T., Walter, U., and Schuh, K. (2005). Gene disruption of Spred-2 causes dwarfism. J. Biol. Chem. *280*, 28572–28580.
55. Messiaen, L., Yao, S., Brems, H., Callens, T., Sathienkijkanchai, A., Denayer, E., Spencer, E., Arn, P., Babovic-Vuksanovic, D., Bay, C., et al. (2009). Clinical and mutational spectrum of neurofibromatosis type 1-like syndrome. JAMA *302*, 2111–2118.
56. Spencer, E., Davis, J., Mikhail, F., Fu, C., Vijzelaar, R., Zackai, E.H., Feret, H., Meyn, M.S., Shugar, A., Bellus, G., et al. (2011). Identification of SPRED1 deletions using RT-PCR, multiplex ligation-dependent probe amplification and quantitative PCR. Am. J. Med. Genet. A. *155A*, 1352–1359.
57. Motta, M., Fidan, M., Bellacchio, E., Pantaleoni, F., Schneider-Heieck, K., Coppola, S., Borck, G., Salviati, L., Zenker, M., Cirstea, I.C., and Tartaglia, M. (2019). Dominant Noonan syndrome-causing LZTR1 mutations specifically affect the Kelch domain substrate-recognition surface and enhance RAS-MAPK signaling. Hum. Mol. Genet. *28*, 1007–1022.
58. Lindeboom, R.G.H., Vermeulen, M., Lehner, B., and Supek, F. (2019). The impact of nonsense-mediated mRNA decay on genetic disease, gene editing and cancer immunotherapy. Nat. Genet. *51*, 1645–1651.
59. Hirata, Y., Brems, H., Suzuki, M., Kanamori, M., Okada, M., Morita, R., Llano-Rivas, I., Ose, T., Messiaen, L., Legius, E., and Yoshimura, A. (2016). Interaction between a Domain of the Negative Regulator of the Ras-ERK Pathway, SPRED1 Protein, and the GTPase-activating Protein-related Domain of Neurofibromin Is Implicated in Legius Syndrome and Neurofibromatosis Type 1. J. Biol. Chem. *291*, 3124–3134.
60. Führer, S., Ahammer, L., Ausserbichler, A., Scheffzek, K., Dunzendorfer-Matt, T., and Tollinger, M. (2017). NMR resonance assignments of the EVH1 domain of neurofibromin's recruitment factor Spred1. Biomol. NMR Assign. *11*, 305–308.
61. Fragale, A., Tartaglia, M., Wu, J., and Gelb, B.D. (2004). Noonan syndrome-associated SHP2/PTPN11 mutants cause EGF-dependent prolonged GAB1 binding and sustained ERK2/MAPK1 activation. Hum. Mutat. *23*, 267–277.
62. Hanna, N., Montagner, A., Lee, W.H., Miteva, M., Vidal, M., Vidaud, M., Parfait, B., and Raynal, P. (2006). Reduced phosphatase activity of SHP-2 in LEOPARD syndrome: consequences for PI3K binding on Gab1. FEBS Lett. *580*, 2477–2482.
63. Motta, M., Sagi-Dain, L., Krumbach, O.H.F., Hahn, A., Peleg, A., German, A., Lissewski, C., Coppola, S., Pantaleoni, F., Kocherscheid, L., et al. (2020). Activating MRAS mutations cause Noonan syndrome associated with hypertrophic cardiomyopathy. Hum. Mol. Genet. *29*, 1772–1783.
64. Anastasaki, C., Estep, A.L., Marais, R., Rauen, K.A., and Patton, E.E. (2009). Kinase-activating and kinase-impaired cardio-facio-cutaneous syndrome alleles have activity during zebrafish development and are sensitive to small molecule inhibitors. Hum. Mol. Genet. *18*, 2543–2554.
65. Runtuwene, V., van Eekelen, M., Overvoorde, J., Rehmann, H., Yntema, H.G., Nillesen, W.M., van Haeringen, A., van der Burgt, I., Burgering, B., and den Hertog, J. (2011). Noonan syndrome gain-of-function mutations in NRAS cause zebrafish gastrulation defects. Dis. Model. Mech. *4*, 393–399.
66. Jindal, G.A., Goyal, Y., Yamaya, K., Futran, A.S., Kountouridis, I., Balgobin, C.A., Schüpbach, T., Burdine, R.D., and Shvartsman, S.Y. (2017). In vivo severity ranking of Ras pathway mutations associated with developmental disorders. Proc. Natl. Acad. Sci. USA *114*, 510–515.
67. Ullrich, M., Aßmus, B., Augustin, A.M., Häbich, H., Abeßer, M., Martin Machado, J., Werner, F., Erkens, R., Arias-Loza, A.P., Umbenhauer, S., et al. (2019). SPRED2 deficiency elicits cardiac arrhythmias and premature death via impaired autophagy. J. Mol. Cell. Cardiol. *129*, 13–26.
68. Kawazoe, T., and Taniguchi, K. (2019). The Sprouty/Spred family as tumor suppressors: Coming of age. Cancer Sci. *110*, 1525–1535.
69. Hanafusa, H., Torii, S., Yasunaga, T., and Nishida, E. (2002). Sprouty1 and Sprouty2 provide a control mechanism for the Ras/MAPK signalling pathway. Nat. Cell Biol. *4*, 850–858.
70. Yusoff, P., Lao, D.H., Ong, S.H., Wong, E.S., Lim, J., Lo, T.L., Leong, H.F., Fong, C.W., and Guy, G.R. (2002). Sprouty2 inhibits the Ras/MAP kinase pathway by inhibiting the activation of Raf. J. Biol. Chem. *277*, 3195–3201.
71. Engelhardt, C.M., Bundschu, K., Messerschmitt, M., Renné, T., Walter, U., Reinhard, M., and Schuh, K. (2004). Expression and subcellular localization of Spred proteins in mouse and human tissues. Histochem. Cell Biol. *122*, 527–538.
72. Inoue, H., Kato, R., Fukuyama, S., Nonami, A., Taniguchi, K., Matsumoto, K., Nakano, T., Tsuda, M., Matsumura, M., Kubo, M., et al. (2005). Spred-1 negatively regulates allergen-induced airway eosinophilia and hyperresponsiveness. J. Exp. Med. *201*, 73–82.
73. Denayer, E., Ahmed, T., Brems, H., Van Woerden, G., Borgesius, N.Z., Callaerts-Vegh, Z., Yoshimura, A., Hartmann, D., Elgersma, Y., D'Hooge, R., et al. (2008). Spred1 is required for synaptic plasticity and hippocampus-dependent learning. J. Neurosci. *28*, 14443–14449.
74. Araki, T., Mohi, M.G., Ismat, F.A., Bronson, R.T., Williams, I.R., Kutok, J.L., Yang, W., Pao, L.I., Gilliland, D.G., Epstein, J.A., and Neel, B.G. (2004). Mouse model of Noonan syndrome

reveals cell type- and gene dosage-dependent effects of Ptpn11 mutation. Nat. Med. *10*, 849–857.

75. Hernández-Porras, I., Fabbiano, S., Schuhmacher, A.J., Aicher, A., Cañamero, M., Cámara, J.A., Cussó, L., Desco, M., Heeschen, C., Mulero, F., et al. (2014). K-RasV14I recapitulates Noonan syndrome in mice. Proc. Natl. Acad. Sci. USA *111*, 16395–16400.
76. Wu, X., Simpson, J., Hong, J.H., Kim, K.-H., Thavarajah, N.K., Backx, P.H., Neel, B.G., and Araki, T. (2011). MEK-ERK pathway modulation ameliorates disease phenotypes in a mouse model of Noonan syndrome associated with the Raf1(L613V) mutation. J. Clin. Invest. *121*, 1009–1025.
77. Ullrich, M., Weber, M., Post, A.M., Popp, S., Grein, J., Zechner, M., Guerrero González, H., Kreis, A., Schmitt, A.G., Üçeyler, N., et al. (2018). OCD-like behavior is caused by dysfunction of thalamo-amygdala circuits and upregulated TrkB/ERK-MAPK signaling as a result of SPRED2 deficiency. Mol. Psychiatry *23*, 444–458.
78. Miraoui, H., Dwyer, A.A., Sykiotis, G.P., Plummer, L., Chung, W., Feng, B., Beenken, A., Clarke, J., Pers, T.H., Dworzynski, P., et al. (2013). Mutations in FGF17, IL17RD, DUSP6, SPRY4, and FLRT3 are identified in individuals with congenital hypogonadotropic hypogonadism. Am. J. Hum. Genet. *92*, 725–743.

The American Journal of Human Genetics, Volume *108*

Supplemental information

SPRED2 loss-of-function causes

a recessive Noonan syndrome-like phenotype

Marialetizia Motta, Giulia Fasano, Sina Gredy, Julia Brinkmann, Adeline Alice Bonnard, Pelin Ozlem Simsek-Kiper, Elif Yilmaz Gulec, Leila Essaddam, Gulen Eda Utine, Ingrid Guarnetti Prandi, Martina Venditti, Francesca Pantaleoni, Francesca Clementina Radio, Andrea Ciolfi, Stefania Petrini, Federica Consoli, Cédric Vignal, Denis Hepbasli, Melanie Ullrich, Elke de Boer, Lisenka E.L.M. Vissers, Sami Gritli, Cesare Rossi, Alessandro De Luca, Saayda Ben Becher, Bruce D. Gelb, Bruno Dallapiccola, Antonella Lauri, Giovanni Chillemi, Kai Schuh, Hélène Cavé, Martin Zenker, and Marco Tartaglia

Supplemental Note: Case Reports

Family 1 (c.1142_1143delTT, p.Leu381Hisfs*95)

Subject 1-II-1

The proband, a 14.7-year-old female, is the second child of consanguineous (first cousins) Turkish parents (father, 27 years and mother, 20 years). The family history was positive for a condition overlapping with that observed in the proband (father, father's sister and maternal uncle). Family tree revealed a high degree of inbreeding. The couple had a first pregnancy characterized by premature delivery at 32 weeks of gestation followed by death in the first day; no additional data are available on the clinical presentation of the newborn. The affected father (1-I-1, see below) exhibits short stature, dysmorphic facial features, short and webbed neck, and hypertrophic cardiomyopathy. The proband was born at term by Caesarean section (breech presentation) after a pregnancy complicated with polyhydramnios with a birth weight of 2,000 g. She required hospitalization for 2 weeks for respiratory distress; however, she did not require mechanical ventilation. She had global developmental delay (head control by 2 months, sit with support by 8 months, sit without support by 12 months, and walked after 22 months of age). She presented with language delay (few words with no sentences by 28 months of age). Psychometric evaluation revealed moderate intellectual disability (IQ 50-69) and learning disorder. She attended special education in infancy. A delay in tooth eruption was documented (after 2 years of age). Hip dysplasia was diagnosed in infancy; however, no intervention was performed in the follow-up. She had failure to thrive and a history of recurrent upper and lower respiratory tract infections. She had strabismus, but no intervention had been performed.

Brain MRI revealed mild left cerebral hemisphere enlargement. Echocardiographic evaluation disclosed mild aortic insufficiency, focal interventricular septum hypertrophy, and mitral valve prolapse. She had lymphopenia, with a lymphocyte activation test documented at the lower border of the normal range. T-cell receptor excision circles (TRECs) and naive T cell number were decreased. She received periodic sulfamethoxazole and trimethoprim prophylaxis. Audiologic evaluation and renal ultrasonography were normal. She had easy bruisability without evidence of coagulation defects. No growth hormone deficiency was shown.

At the last evaluation (14.2 years), weight was 42 kg (-1.02 SD), height was 145 cm (-2.41 SD), and head circumference was 57 cm (+1.32 SD). Her craniofacial appearance was characterized by a triangular face, bitemporal narrowing, hypertelorism, mild ptosis, low-set and posteriorly rotated ears with helix folding anomaly and a dysmorphic ear lobe, prominent nasal bridge, low posterior hairline and short/webbed neck. Pectus excavatum and cubitus valgus were also present.

Subject 1-I-1

The affected father is a 40 year-old individual. He has mild intellectual disability but no formal psychometric evaluation had been performed. The educational level was low; learning disabilities were reported. Echocardiographic evaluation revealed class II hypertrophic cardiomyopathy.

At last evaluation (40 years), weight was 56 kg (-1.29 SD), height was 144 cm (-4.35 SD), and head circumference was 56 cm (-1 SD). The craniofacial appearance was characterized by a triangular face, bitemporal narrowing, down-slanted palpebral fissure, low-set and posteriorly rotated ears,

prominent nasal bridge, long philtrum, prominent naso-labial folds, low posterior hairline, and short and webbed neck. Cubitus valgus and mild pectus excavatum were present as well.

Family 2 (c.299T>C, p.Leu100Pro)

Subject 2-II-1

The proband is an 8-year-old boy, second child of apparently healthy, consanguineous (first-degree cousins) Turkish parents. He has two healthy sibs (one brother and one sister) and no affected relative. The family was first referred to our department for genetic counseling because cystic hygroma, polyhydramnios, unilateral ventriculomegaly and renal pelviectasis were identified by ultrasonography (16th week of gestation). The nuchal fold was 8.2 mm. Chromosome analysis of amniocytes showed normal results. He was born on 37th week of gestation with a birth weight of 3,280 g. Neonatal intensive care was required for one week due to late sepsis. On his first examination, he had a coarse face, macrocephaly, wide anterior fontanelle, high forehead, down-slanting palpebral fissures, bilateral epicanthus and hypertelorism, depressed and prominent nasal bridge, low-set posteriorly rotated ears with anterior facing large earlobes, low posterior hairline, webbed neck, wide and short thoracic cage, right cryptorchidism, and loose skin. First echocardiography assessment documented asymmetrical hypertrophy of interventricular septum (7 mm), while trans-fontanelle ultrasonography revealed mild left ventriculomegaly. Diagnosis of Noonan syndrome was posed. *PTPN11* mutation analysis was negative, as well as mutation scan of the other known RASopathy genes.

At follow-up, he showed mild developmental delay (he walked at 19 months), and intellectual disability, and required educational assistance at school. He had atopic complaints with a runny nose and ectodermal problems during infancy (itchy, eczematous skin, dry and scaly skin on face and extensor surfaces of arms and legs). He also had sparse eyebrows and eyelashes with sparse curly and lighter colored hair than his family, loose and thick skin. Immunological tests were normal. He was operated for bilateral nasolacrimal duct stenosis, bilateral exotropia and bilateral cryptorchidism in the first 2 years of his life. He had asymmetrical septal hypertrophy, atrial septal defect (ostium secundum) and pulmonary valvular stenosis. He required pulmonary balloon valvuloplasty (1 year of age). Sharp wave pattern and organization defect on EEG was documented during the second year of his life without occurrence of seizures.

At 2 years of age, brain MRI and control EEG were unremarkable. He had a long aPTT and his coagulation factor XII activity was 24.8%, not requiring treatment. His pectus deformity worsened over time. He had typical pectus carinatum superiorly and pectus excavatum inferiorly; he also had mild pes valgus and planus bilaterally. At 3 and half years, renal ultrasonography revealed grade 2 medullary nephrocalcinosis. His height was between 10th and 25th percentiles, and weight was between 25th and 50th percentiles.

At his last examination, he complained widespread bone pain and myalgia. Laboratory tests were normal. Dysmorphological assessment highlighted an oval face, hypertelorism, downward slanted palpebral fissures, ptosis, prominent glabella, anteverted nares, prominent philtrum, receding chin, low-set ears, folded helix, short webbed neck, pectus carinatum/excavatum, teletelia, kyphosis, and winged shoulder blades.

Family 3 (c.187C>T, p.Arg63*)

Subject 3-II-1

The proband is an 11-year-old Tunisian girl born to consanguineous parents (first-degree cousins). She was referred for a first evaluation at the age of 2.7 years because of splenomegaly. She is the product of an uneventful pregnancy. Delivery occurred by Caesarean section because of macrosomia (birth weight = 4,100 Kg [+2 SD], birth height = 50 cm [0 SD], head circumference = 35.5 cm [+0.5 SD]). Apgar scores were 8, 9, and 10 at 1, 5, and 10 minutes, respectively. The child had moderate pulmonary valve stenosis (30 mmHg), which was discovered at 2 months and confirmed by ultrasound assessment at the age of 2 months and 4 years. The developmental milestones were delayed.

At our first clinical examination, weight was 14 kg (+1 SD), height was 81 cm (-3 SD), and head circumference was 53 cm (+3 SD), with dolichocephaly. A coarse face, relative macrocephaly, high forehead, bitemporal constriction, triangular face, hypertelorism, downslanting palpebral fissures, ptosis of the left eye with convergent strabismus, low-set ears (without posterior rotation and thickening of the ear lobes), prominent nasal bridge, anteverted nostrils, long philtrum, thick lips, high-arched palate with narrow palate, microretrognathia, and pterygium colli with low posterior hairline were noticed. Pectus excavatum with widely-spaced nipples, bilateral clinodactyly of the 4th and 5th fingers, bilateral toe malposition suggestive of diapason-shaped toes, as well as articular hyperlaxity and kyphosis were present. Neurological examination found attention deficit and slight psychomotor delay. Systolic murmur on auscultation was also noted; an ECG and a Holter monitor recording revealed atrial and ventricular extrasystoles. An echocardiogram at age 9.5 years confirmed the moderate pulmonary valve stenosis and revealed moderate mitral regurgitation. Multiple audiograms were normal. Abdominal evaluation revealed splenomegaly reaching the umbilical area without hepatomegaly. Hirsutism of the upper part of the back, and hyperhidrosis were present. Laboratory tests found a mild microcytic hypochromic anemia with normal hemoglobin electrophoresis. A slight increase in serum levels of FT4 with normal levels of TSH.

A follow-up at the age of 9.3 years showed that the proband had skills within lower limits for the age without a defined cognitive deficit. Height was within the normal range while weight was under normal range. She had enuresis and encopresis. Recurrent infections affecting ears (seromucous otitis) and lungs (bronchitis) were reported. The splenomegaly had spontaneously regressed. Chronic constipation was linked to a sigmoid dolichocolon discovered on X-rays.

At our most recent follow-up (11.9 years), height was 136.5 cm (-1.5 SD), weight was 27.5 kg (-2.3 SD), and head circumference was 55cm (+1 SD). She failed her 5th grade school exams.

Karyotype was normal. A diagnosis of Noonan syndrome was suspected, which was not confirmed molecularly.

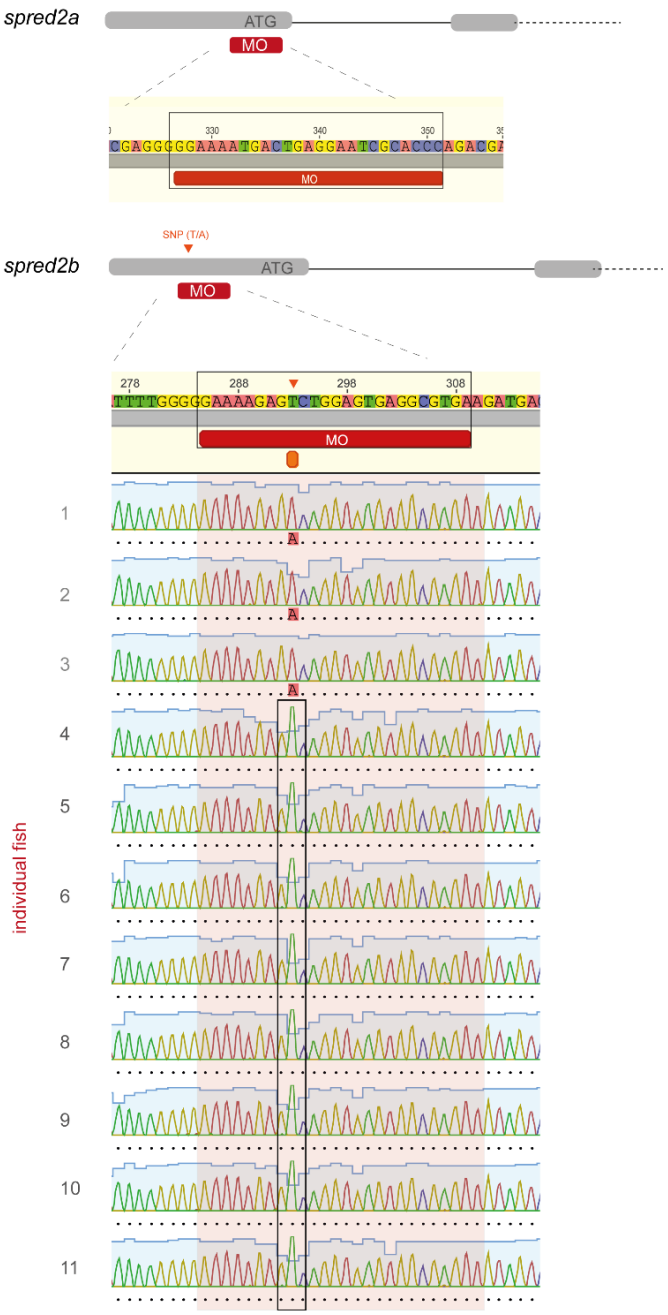

Figure S1. *spred2a* and *spred2b* ATG-MO design and genotyping of the target genomic sequence.

Scheme showing the MO design and target sequence on the 5'-UTR/ATG region of zebrafish *spred2a* and *spred2b* genes. A SNP (T/A) is annotated in the target region of *spred2b* (orange arrowhead). To ensure homogeneous efficiency of the MO-mediated knockdown, Sanger sequencing was performed to select proper genotypes for mating. Chromatograms of the relevant genomic region from individual NHGRI zebrafish embryos are shown in the lower panel. Fish having the "T" allele matching the sequence used to target *spred2b* are outlined by a black line.

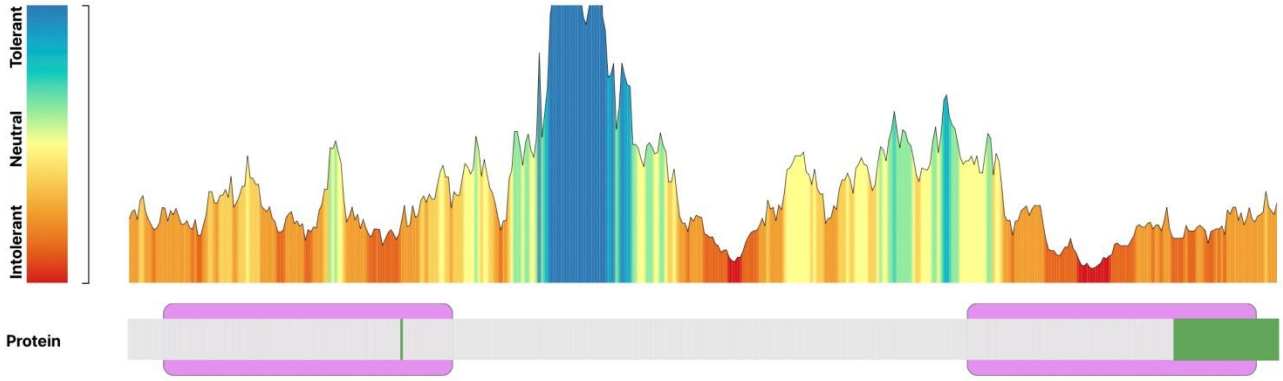

Figure S2. Tolerance landscape of genetic variation for *SPRED2*.

The histograms show the non-synonymous over synonymous (d_N/d_S) ratio for individual residues, as calculated by MetaDome, which are colored according to the scheme reported along the Y-axis. The protein sequence is depicted in grey with the EVH1 (*N*-terminus, left) and SPR (*C*-terminus, right) domains shown in violet. Leu^{100} and the region *C*-terminal to Leu^{381} affected by two of the three homozygous disease-causing variants identified in the study are shown in green. The two pathogenic variants affect two intolerant regions of the protein.

Figure S3. Multiple alignment of the stretches of the EVH1 and SPR domains encompassing Leu^{100} and Leu^{381} of SPRED2 in orthologs and human paralogs.

Position of Leu^{100} and Leu^{381} are indicated (red arrows). The c.1142_1143delTT frameshift at codon 381 was predicted to result in an extended open reading frame characterized by a divergent *C*-terminal tail lacking key residues of the protein required for SPRED2 palmitoylation, a posttranslational modification required for proper targeting of the protein to the plasma membrane. The resulting variant amino acid sequence is above the alignment. Invariant residues among proteins are highlighted in black (consensus > 70%); gray background indicates residues similar to consensus amino acid (grouped as FYW, ILVM, DE, GA, ST, RQ, RKH).

Alignment was generated using MUSCLE v3.8 and visualized by means of pyBoxshade v1.2. SPRED2: *H. sapiens*, NP_861449.2; *M. musculus*, NP_277058.1; *B. Taurus*, XP_005212957.1; *G. gallus*, XP_419341.3; *D. rerio*, NP_998399.1; *X. tropicalis*, NP_001011032.1; *D. melanogaster*, NP_610988.1; SPRED1: *H. sapiens*, NP_689807.1; SPRED3: *H. sapiens*, XP_006723282.1.

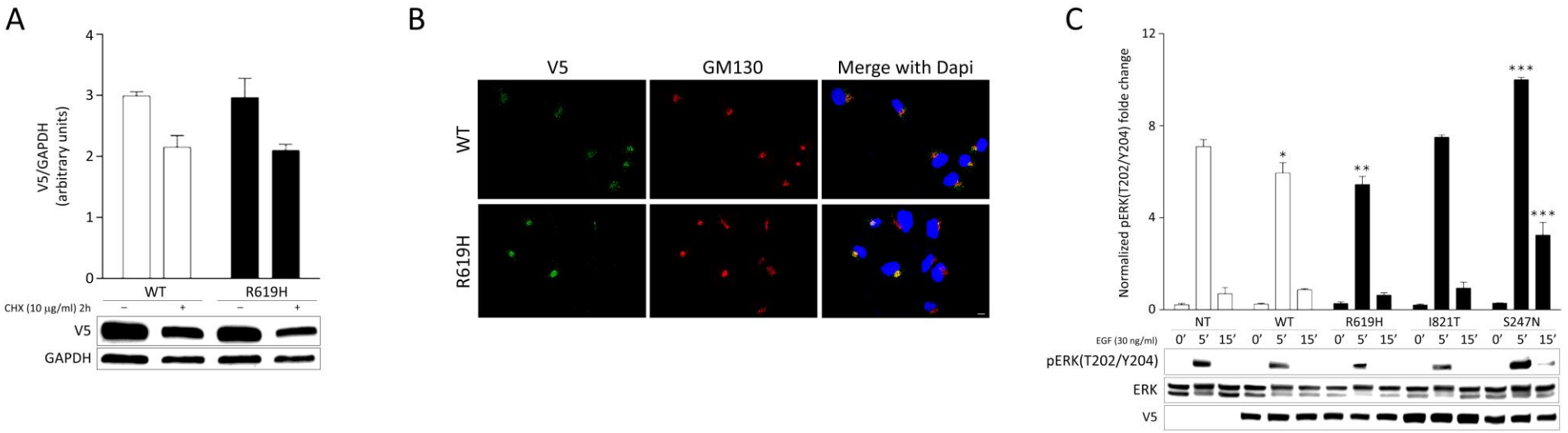

Figure S4. Biochemical and functional characterization of the LZTR1^{Arg619His} protein.

The variant *LZTR1* cDNA was transiently overexpressed in COS-1 cells and tested for stability (A), subcellular localization (B) and impact on pERK levels (C). Previous studies demonstrated that the inactivating *LZTR1* variants implicated in recessive NS cause accelerated degradation or aberrant subcellular localization of LZTR1. When overexpressed, differently from the WT protein, these variants do not downmodulate pERK levels following EGF stimulation. In contrast, dominant negative *LZTR1* variants result in enhanced phosphorylation of ERK following EGF stimulation.

(**A**) Protein levels of the V5-tagged WT and variant (R619H) LZTR1 proteins in transfected COS-1 cells, basally and after CHX (10 µg/mL) treatment. Representative blots and mean ± SD densitometry values of three independent experiments are shown. GAPDH was used as a loading control.

(**B**) Subcellular localization of transiently expressed V5-tagged LZTR1 proteins in COS-1 cells revealed by confocal microscopy analysis. Similar to WT LZTR1, LZTR1^{Arg619His} (R619H) is localized at the level of the Golgi. Cells were stained with the anti-V5 monoclonal antibody (green). Co-localization analysis was performed using the *cis*-Golgi marker GM130 (red). Merged images are shown in the right panels. Scale bar, 10 µm.

(**C**) Similar to the WT protein, LZTR1^{Arg619His} (R619H) weakly but significantly downmodulates ERK phosphorylation when compared with NT (mock transfection) in HEK 293T cells. Overexpression of the recessive NS-causing LZTR1^{Ile821Thr} (I821T) protein fails in modulating ERK phosphorylation, while expression of dominantly acting LZTR1^{Ser247Asn} (S247N) promotes enhanced ERK phosphorylation. Representative blots (below) and mean ± SD densitometry values (above) of three experiments are shown. Asterisks indicate statistically significant differences compared with NT (mock transfection) at the corresponding time upon EGF stimulation (*$P < 0.05$; ** $P < 0.005$; *** $P < 0.001$; two-way ANOVA followed by Tukey's multiple comparison test).

The three assays consistently indicate that the p.Arg619His change does not significantly impact LZTR1 function and MAPK signaling.

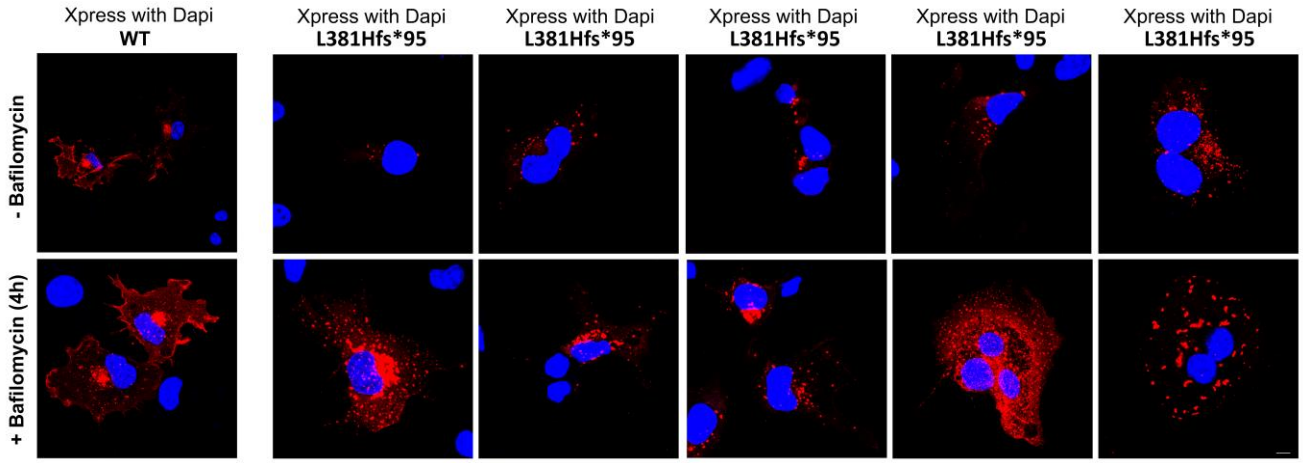

Figure S5. Bafilomycin treatment rescues the accelerated degradation of SPRED2^{Leu381Hisfs*95}.

SPRED2^{Leu381Hisfs*95} (L381Hfs*95) protein accumulates in vesicular structures suggesting its degradation *via* lysosomes. Subcellular localization of transiently expressed Xpress-tagged wild-type and mutated SPRED2 proteins in COS-1 cells under basal conditions and after bafilomycin A1 (200 nM, 4 h) treatment revealed by confocal microscopy analysis. Cells were stained with an anti-Xpress monoclonal antibody and Alexa Fluor 594 goat anti-mouse secondary antibody (red). Merged images with nuclei (DAPI staining, blue) are displayed. Scale bar, 10 μm.

Bafilomycin was used to inhibit autophagy and lysosomal protein degradation (bottom panel). As shown, the treatment resulted in the accumulation of puncta, which likely represent autophagosomes and lysosomes. Differently from the wild-type protein (WT), SPRED2^{Leu381Hisfs*95} does not localize at the plasma membrane.

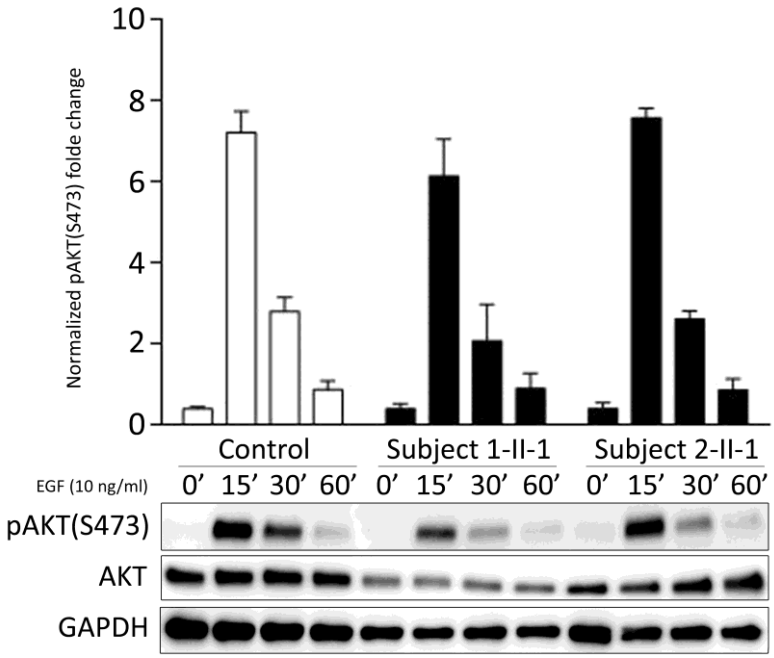

Figure S6. Defective SPRED2 function does not perturb signaling through the PI3K-AKT pathway.

Primary fibroblasts from subjects 1-II-1 (p.Leu381Hisfs*95) and 2-II-1 (p.Leu100Pro) show levels of AKT phosphorylation, basally and after EGF stimulation, that are comparable to those of control cells. Fibroblasts were starved for 16 h and then stimulated with EGF (10 ng/mL), in time-course experiments, or left unstimulated. Equal amounts of cell lysates were resolved on 7.5% polyacrylamide gel. Representative blots (below) and graphs reporting mean ± SD densitometry values (above) of three independent experiments are shown.

These findings are consistent with previous observations indicating that SPRED proteins do not participate in the control of PI3K-AKT signaling.

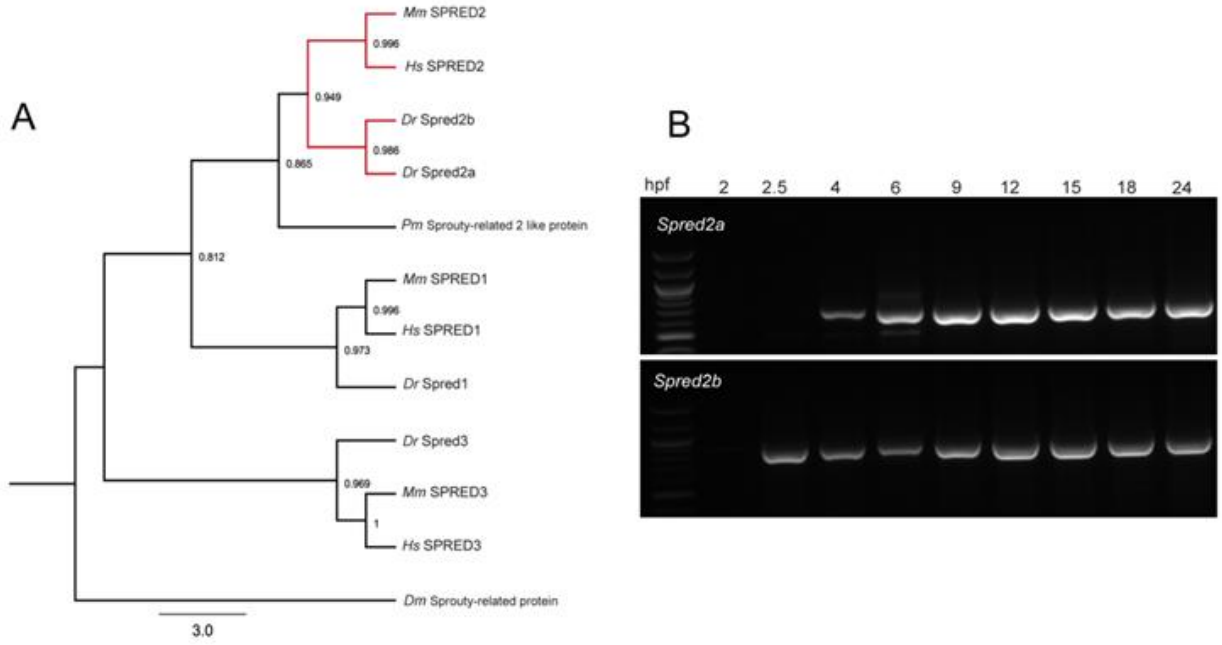

Figure S7. Zebrafish *spred2a* and *spred2b* paralogs, and their expression during early phases of development.

(A) Phylogenetic analysis of the spred2 paralogs (*Dr*, *Danio rerio*) compared to the human (*Hs*, *Homo sapiens*) and mouse (*Mm*, *Mus musculus*) orthologs and paralogs. Sequence data were retrieved from Ensemble. Sequence alignment was generated using Muscle 3.8. Maximum likelihood trees were generated using PhyML 3.0 with the LG substitution model and 100 bootstrap replicates. *Pm*, *Petromyzon marinus*; *Dm*, *Drosophila melanogaster.* Statistical support per node is shown.

(B) RT-PCR showing the expression profile of zebrafish *spred2a* and *spred2b* during early embryogenesis (2-24 hpf, hours post-fertilization).

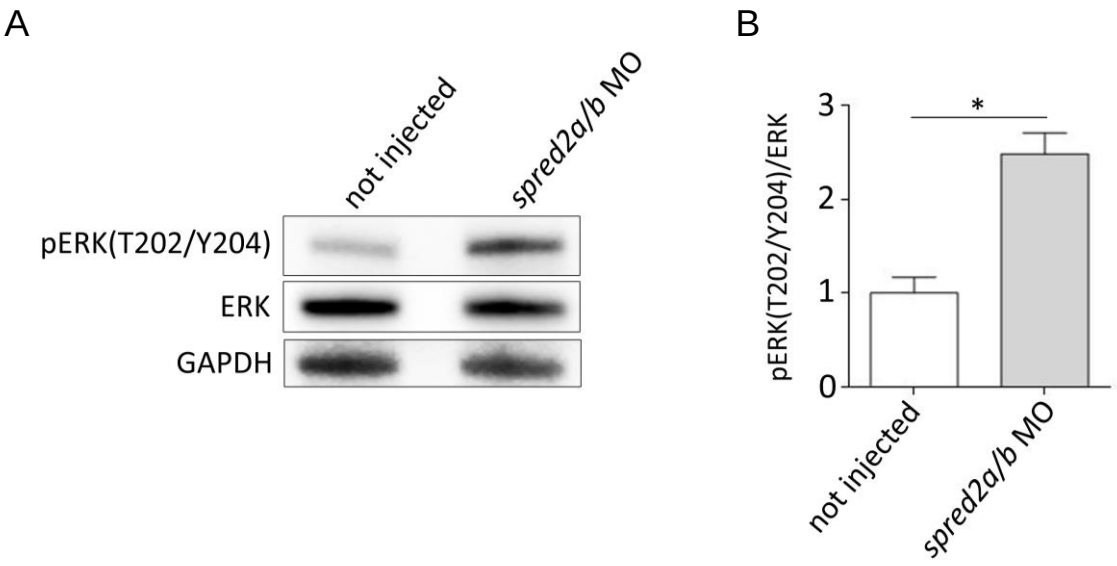

Figure S8. Enhanced Erk phosphorylation in zebrafish embryos injected with *spred2a* and *spred2b* antisense oligonucleotides (MO).

Representative blots (A) and graph reporting mean ± SEM densitometry values (B) of two independent experiments are shown. The asterisk indicates a statistically significant higher Erk phosphorylation level in morphants compared with non-injected embryos (Student's t-test, * indicates $P < 0.05$).

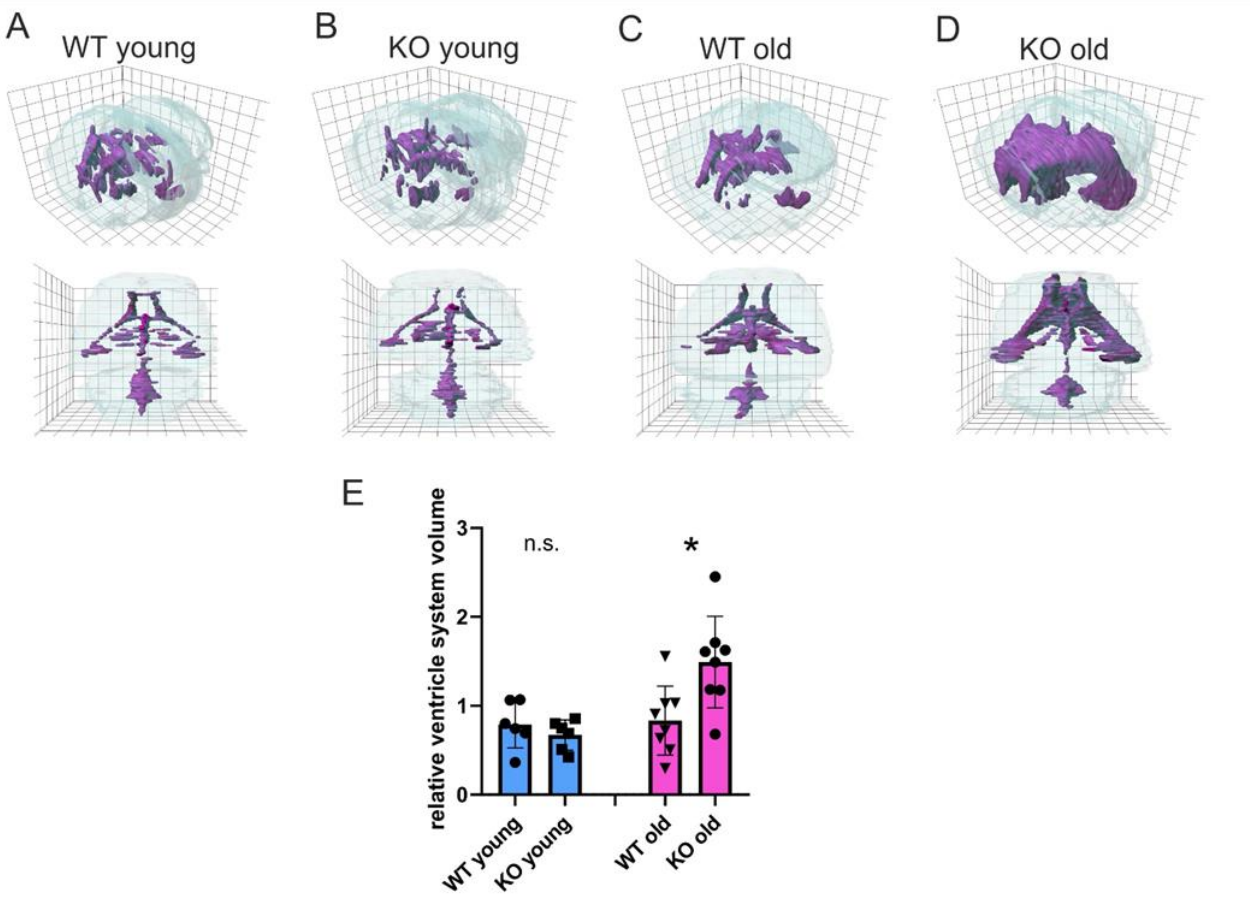

Figure S9. Enlarged brain ventricles in aged *Spred2* KO mice.

(**A**) 3D model of a reconstructed mouse brain ventricular system of a young (6-12 weeks) WT mouse.

(**B**) 3D model of a reconstructed mouse brain ventricular system of a young (6-12 weeks) *Spred2* KO mouse.

(**C**) 3D model of a reconstructed mouse brain ventricular system of an old (12 months) WT mouse.

(**D**) 3D model of a reconstructed mouse brain ventricular system of an old (12 months) *Spred2* KO mouse.

(**E**) Quantification of ventricle system volumes in relation to whole brain volumes (n = 6 in each young group, n = 8 in each old group; * indicates $P < 0.05$).

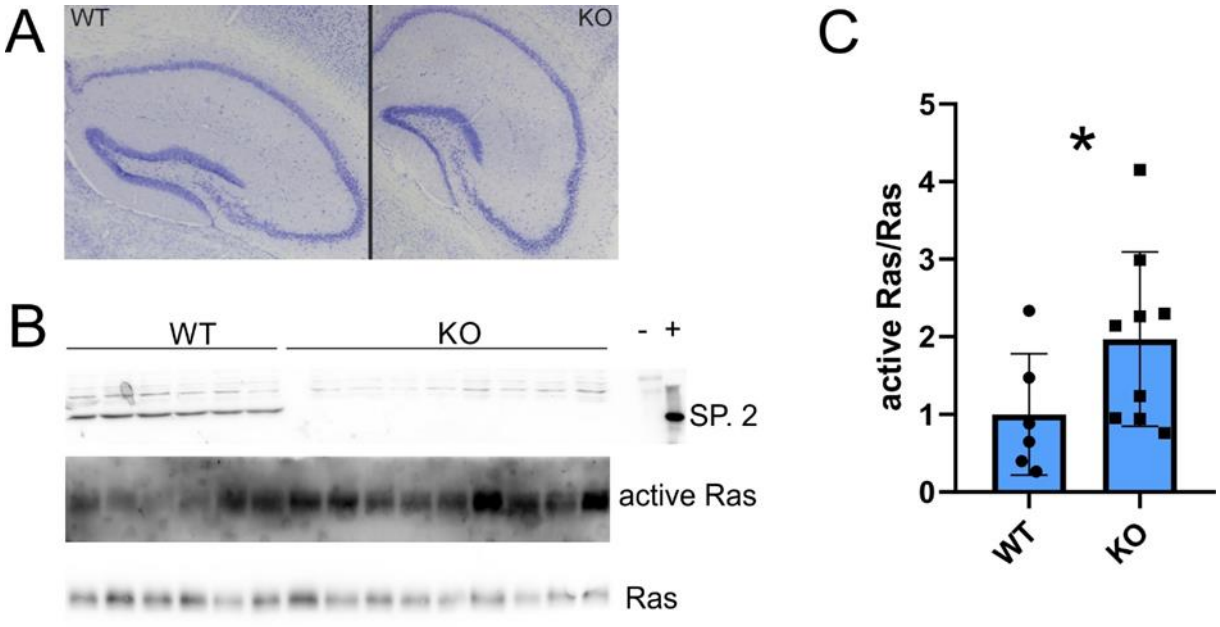

Figure S10. Increased Ras activity in hippocampus of *Spred2* KO mice.

(**A**) Micrographs of Nissl-stained hippocampus regions of a WT mouse in comparison to an age-matched *Spred2* KO mouse. The hippocampus of the KO mice appears compressed and not fully developed, particularly at the structure of the gyrus dentatus.

(**B**) Western blot analysis of hippocampus lysates showing Spred2 levels in WT mice and lack of the protein in *Spred2* KO mice (top). "-" and "+" indicate non-transfected and pCMV-*SPRED2*-transfected HEK 293T cell lysates serving as negative and positive controls, respectively. Middle and lower panels show western blots of pulled-down GTP-bound Ras and levels of total Ras in hippocampus lysates, respectively.

(**C**) Quantification of GTP-bound Ras:total Ras ratio in hippocampus of *Spred2*$^{+/+}$ and *Spred2*$^{-/-}$ mice aged six to twelve months. (WT mice, n = 6; *Spred2* KO mice, n = 9; * indicates $P < 0.05$).

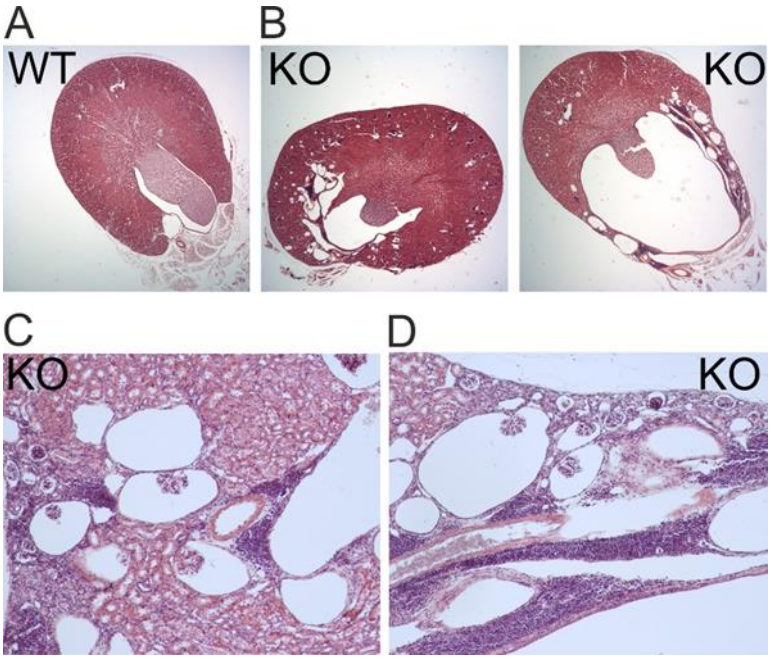

Figure S11. Signs of hydronephrosis and polycystic kidneys in *Spred2* KO mice.

(**A**) Hematoxylin-eosin (HE) stained section of kidney from a WT mouse demonstrating normal structure, no appearance of cysts, and a narrow renal pelvis.

(**B**) Examples of HE stained sections of kidneys from a *Spred2* KO mouse. In these, the renal pelvises were found to be dilated, the renal macroscopic structure was disturbed, and various cysts were visible.

(**C, D**) Higher magnifications revealed multiple cystic formations, expanded Bowman`s capsules, and lymphocyte infiltration in kidneys of *Spred2* KO mice.

Table S1. Clinical features of the disorder caused by SPRED2 LoF compared with neurofibromatosis type 1, Legius syndrome and Noonan syndrome.

Feature	NF1	Legius syndrome	*SPRED2*-related disorder	NS
CALMs	++	++	-	+/-
Freckling	++	++	-	-
Macrocephaly	+	+	+	+
NS-like facial features	+/-	+/-	++	++
Short/webbed neck	+/-	+/-	++	++
Short stature	+/-	+/-	+	++
PVS	+/-	-	+	+
HCM	-	-	+	+
ID	+/-	-	++	+/-
Learning difficulties	++	+	+	+
Lisch nodules	++	-	-	-
neurofibroma	++	-	-	-
Malignant peripheral nerve sheath tumors	+/-	-	-	-
Optic pathway glioma	+	-	-	-
Skeletal defects	sphenoid wing dysplasia, pseudoarthrosis	-	chest defects	chest defects
Inheritance	D	D	R	D/R

D, dominant; R, recessive.